Journal of Molecular and Cellular Cardiology 124 (2018) 12–25

Contents lists available at ScienceDirect

Journal of Molecular and Cellular Cardiology

journal homepage: www.elsevier.com/locate/yjmcc

Distinct patterns of atrial electrical and structural remodeling in angiotensin II mediated atrial fibrillation

Hailey J. Jansen[a], Martin Mackasey[a], Motahareh Moghtadaei[b], Darrell D. Belke[a], Emmanuel E. Egom[b,1], Jari M. Tuomi[c], Sara A. Rafferty[b], Adam W. Kirkby[a], Robert A. Rose[a,*]

[a] Libin Cardiovascular Institute of Alberta, Department of Cardiac Sciences, Department of Physiology and Pharmacology, Cumming School of Medicine, University of Calgary, Calgary, Alberta, Canada
[b] Department of Physiology and Biophysics, Faculty of Medicine, Dalhousie University, Halifax, Nova Scotia, Canada
[c] Department of Medicine, Schulich School of Medicine & Dentistry, Western University, London, Ontario, Canada

ARTICLE INFO

Keywords:
Atrial fibrillation
Angiotensin II
Action potential
Na^+ current
K^+ current
Fibrosis

ABSTRACT

Atrial fibrillation (AF) is prevalent in hypertension and elevated angiotensin II (Ang II); however, the mechanisms by which Ang II leads to AF are poorly understood. Here, we investigated the basis for this in mice treated with Ang II or saline for 3 weeks. Ang II treatment increased susceptibility to AF compared to saline controls in association with increases in P wave duration and atrial effective refractory period, as well as reductions in right and left atrial conduction velocity. Patch-clamp studies demonstrate that action potential (AP) duration was prolonged in right atrial myocytes from Ang II treated mice in association with a reduction in repolarizing K^+ currents. In contrast, APs in left atrial myocytes from Ang II treated mice showed reductions in upstroke velocity and overshoot, as well as greater prolongations in AP duration. Ang II reduced Na^+ current (I_{Na}) in the left, but not the right atrium. This reduction in I_{Na} was reversible following inhibition of protein kinase C (PKC) and PKCα expression was increased selectively in the left atrium in Ang II treated mice. The transient outward K^+ current (I_{to}) showed larger reductions in the left atrium in association with a shift in the voltage dependence of activation. Finally, Ang II caused fibrosis throughout the atria in association with changes in collagen expression and regulators of the extracellular matrix. This study demonstrates that hypertension and elevated Ang II cause distinct patterns of electrical and structural remodeling in the right and left atria that collectively create a substrate for AF.

1. Introduction

Atrial fibrillation (AF) is highly prevalent in the setting of hypertension, where 60–80% of individuals with AF also have high blood pressure [1]. Hypertension, which affects > 30% of the global population (i.e. > 1.3 billion people) [2,3], is associated with activation of the renin-angiotensin system and elevated angiotensin II (Ang II) and has been linked to AF [4–7]. Nevertheless, the mechanisms by which hypertension and Ang II lead to AF are complex and incompletely understood. As a result, current therapeutic approaches for AF, which remains the most commonly encountered cardiac arrhythmia [5], are limited and patients with AF remain at risk for stroke and heart failure

Abbreviations: 4-AP, 4 aminopyridine; ACE2, angiotensin converting enzyme 2; AERP, atrial effective refractory period; AF, atrial fibrillation; Ang II, angiotensin II; AP, action potential; APD_{20}, action potential duration at 20% repolarization; APD_{50}, action potential duration at 50% repolarization; APD_{70}, action potential duration at 70% repolarization; APD_{90}, action potential duration at 90% repolarization; AVERP, atrioventricular node effective refractory period; BIM1, bisindolylmaleimide 1; CaMKII, Ca^{2+}/calmodulin-dependent protein kinase II; CV, conduction velocity; EAD, early afterdepolarization; G_{max}, maximum conductance; $I_{Ca,L}$, L-type calcium current; I_{Kur}, ultra-rapid delayed rectifier potassium current; I_{Kr}, rapid delayed rectifier potassium current; I_{Ks}, slow delayed rectifier potassium current; I_{Kss}, steady state potassium current; I_{Na}, sodium current; I_{to}, transient outward potassium current; IV relationship, current-voltage relationship; KChIP2, K^+ channel interacting protein 2; LA, left atrium; MMP, matrix metalloproteinase; OS, overshoot; PKC, protein kinase C; RA, right atrium; RMP, resting membrane potential; SR, sarcoplasmic reticulum; TIMP, tissue inhibitor of metalloproteinase; TGFβ, transforming growth factor β; V_{max}, maximum upstroke velocity; $V_{1/2(act)}$, voltage for 50% channel activation

* Corresponding author at: Libin Cardiovascular Institute of Alberta, Cumming School of Medicine, University of Calgary, GAC66, Health Research Innovation Centre, 3280 Hospital Drive N.W., Calgary, Alberta T2N 4Z6, Canada.
E-mail address: robert.rose@ucalgary.ca (R.A. Rose).
[1] Present address: Department of Medicine, St. Martha's Regional Hospital, Antigonish, Nova Scotia, Canada.

https://doi.org/10.1016/j.yjmcc.2018.09.011
Received 21 August 2018; Received in revised form 25 September 2018; Accepted 26 September 2018
Available online 28 September 2018

as well as a compromised quality of life.

AF is thought to occur due to triggered activity in the setting a proarrhythmic substrate [5,8]. A substrate for AF may be created due to electrical and/or structural remodeling in the atria. The morphology of the atrial action potential (AP) is a critical determinant of atrial electrophysiology and alterations in AP morphology due to electrical remodeling can contribute to the initiation and/or maintenance of AF [5]. Specifically, the upstroke of the AP, which is determined by the Na^+ current (I_{Na}, carried by $Na_V1.5$ channels) [9] is a major determinant of conduction velocity [10]. Changes in atrial I_{Na} and AP upstroke velocity can affect atrial conduction velocity and thus the wavelength of reentry (defined as the product of conduction velocity and atrial refractory period) [5]. Repolarization of the AP is affected by the balance between a number of ionic currents, including the L-type Ca^{2+} current ($I_{Ca,L}$) [9] and several K^+ currents such as the transient outward K^+ current (I_{to}, carried by $K_V4.2/4.3$ channels), the ultra rapid delayed rectifier K^+ current (I_{Kur}, carried by $K_V1.5$ channels), a steady state K^+ current (I_{Kss}, carried by $K_V2.1$ channels) and, depending on species, rapid and slow components of the delayed rectifier K^+ current (I_{Kr} and I_{Ks}) [11]. Alterations in one or more of these currents can impair repolarization (i.e. prolong the AP) and cause triggered activity in the form of early afterdepolarizations (EADs), which can initiate AF [5].

In addition to electrical remodeling in atrial myocytes, a substrate for AF can also arise due to structural remodeling in association with increases in atrial size and atrial fibrosis [5]. Enhanced fibrosis, which can occur in association with an increase in collagen deposition or alterations in extracellular matrix remodeling by matrix metalloproteinases (MMPs) and their inhibitors (TIMPs) [12], can be proarrhythmic because fibrosis can disrupt connectivity between myocytes and impair normal electrical conduction, thereby decreasing the wavelength of reentry [13].

The goal of the present study was to investigate atrial electrophysiology and the basis for AF in the setting of hypertension induced by elevated Ang II. Our data demonstrate that Ang II treated mice are highly susceptible to induced AF in association with impaired atrial conduction. Impaired conduction occurred due to distinct patterns of electrical and structural remodeling in the right and left atria.

2. Methods

An expanded Methods section is provided in the Data Supplement.

2.1. Mice

This study used male wildtype C57Bl/6 mice between the ages of 10–15 weeks. Mice were treated with saline or Ang II (3 mg/kg/day) for 3 weeks using osmotic minipumps (Alzet) implanted subcutaneously. All experimental procedures were approved by the University of Calgary Animal Care and Use Committee and the Dalhousie University Committee for Laboratory Animals and were in accordance with the guidelines of the Canadian Council on Animal Care.

2.2. Blood pressure and echocardiography

Blood pressure was measured in conscious, restrained mice by tail-cuff plethysmography (IITC Life Sci). Cardiac structure was assessed by echocardiography in mice anesthetized by isoflurane inhalation (2%) using a Vevo 3100 ultrasound machine (Fujifilm VisualSonics).

2.3. In vivo electrophysiology and arrhythmia studies

Surface ECGs were measured in anesthetized mice (2% isoflurane inhalation) using 30 gauge subdermal needle electrodes (Grass Technologies). In conjunction, a 1.2F octapolar electrophysiology catheter (Transonic) was inserted into the right heart via an incision in the jugular vein and used to assess inducibility of AF during burst pacing [14,15]. AF was defined as a rapid and irregular atrial rhythm (fibrillatory baseline in the ECG) with irregular RR intervals lasting at least 1 s on the ECG. AF was categorized into three groups: < 5 s (brief); 5–30 s (non-sustained); > 30s (sustained) in order to assess severity of AF when induced, as has been done previously [15,16]. Atrial and AV node effective refractory periods (AERP, AVERP) were measured using S1-S2 pacing protocols in which the heart was paced at a cycle length of 100 ms (S1) followed by an extra stimulus (S2) at progressively shorter cycle lengths as previously described [14,15]. Correct catheter placement was ensured by obtaining a sole ventricular signal in the distal lead and predominant atrial signal in the proximal lead. Body temperature was maintained at 37 °C using a heating pad for these studies. Additional details are provided in the Data Supplement.

2.4. High resolution optical mapping

To study activation patterns and electrical conduction in the atria, high resolution optical mapping was performed in isolated atrial preparations using methods we have described in detail previously [14,17–19]. Atrial preparations were immobilized using blebbistatin (10 μM) [20]. Changes in fluorescence were captured using the voltage sensitive dye Di-4-ANEPPS (10 μM) and a high speed EMCCD camera at ~900 frames/s. Spatial resolution was 67 × 67 μm/pixel. All experiments were performed at 35 °C. Data were analyzed using custom software written in Matlab. Further details are available in the Data Supplement.

2.5. Patch-clamping of isolated atrial myocytes

Right and left atrial myocytes were isolated from mice by enzymatic digestion as we have described previously [21,22]. These myocytes were used to record APs using the perforated patch-clamp technique or the whole cell patch-clamp technique. I_{Na}, I_K, and $I_{Ca,L}$ were recorded using the whole cell patch-clamp technique. The solutions and experimental protocols for each of these approaches are available in the Data Supplement.

2.6. Western blotting

Right and left atrial samples were used to measure the protein expression of protein kinase Cα (PKCα), $K_V4.2$, $K_V4.3$, $K_V1.5$ and KChIP2 as well as GAPDH as the loading control. The procedures for these experiments are provided in the Data Supplement.

2.7. Quantitative PCR

Quantitative gene expression was measured in the right and left atria as we have previously described [14,15]. Intron spanning primers for SCN5a ($Na_V1.5$), KCND2 ($K_V4.2$), KCND3 ($K_V4.3$) and KCNIP2 (KChIP2), KCNA5 ($K_V1.5$) Col1a2 (collagen type I), Col3a1 (collagen type III), transforming growth factor β (TBFβ), matrix metalloproteinases 2 and 9 (MMP2, MMP9) and tissue inhibitor of metalloproteinases 1–4 (TIMP1, TIMP2, TIMP3, TIMP4) as well as GAPDH and β-actin (reference genes) were used. Experimental protocols and primer sequences are in the Data Supplement.

2.8. Collagen staining and collagen assay

Interstitial collagen was assessed using picrosirius red (collagen) and fast green (myocardium) staining of paraffin embedded sections (3 μm) through the right and left atria. The level of fibrosis was quantified using ImageJ software as previously described [14,15]. Total collagen content was measured in right and left atria using a hydroxyproline assay (Sigma-Aldrich) according to kit instructions.

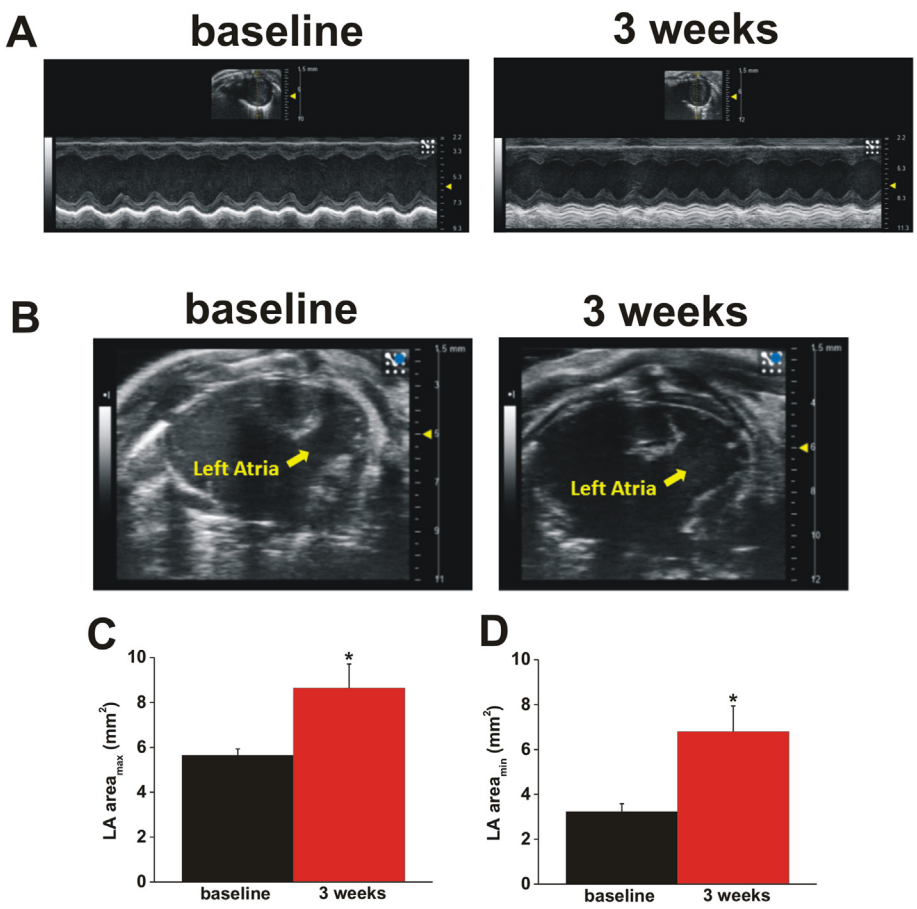

Fig. 1. Echocardiography in mice treated with Ang II. **A**, Representative M-mode images measured from the short axis at baseline and after 3 weeks of Ang II treatment. Refer to Supplemental Table 1 for a summary of echocardiography measurements. **B**, Representative images used to assess left atrial area in Ang II treated mice. Bars on left side of panels A and B represent contrast intensity. Scale bars on right side of panel A and B are measures of distance in mm. **C and D**, Summary of the effects of Ang II on left atrial maximum (**C**) and minimum (**D**) area. *$P < 0.05$ vs. baseline by Student's *t*-test; $n = 5$ mice per group.

2.9. Statistical analysis

All data are presented as means ± SEM. Data were analyzed using Fischer's exact test, Student's *t*-test, two-way ANOVA with Tukey's posthoc test or two-way repeated measures ANOVA with Tukey's posthoc test as indicated in each figure legend. $P < 0.05$ was considered significant.

3. Results

3.1. Effects of Ang II on atrial structure and atrial arrhythmogenesis

Initially, we measured the effects of Ang II treatment on blood pressure and cardiac structure and function. Supplemental Fig. S1 demonstrates that 3 weeks of Ang II treatment increased ($P < 0.05$) systolic and diastolic blood pressure while saline treated controls exhibited no differences ($P = 1.00$) in blood pressure. Echocardiography assessment (Fig. 1A, Supplemental Table 1) demonstrates that Ang II treatment caused a hypertrophic response characterized by an increase ($P < 0.05$) in thickness of the left ventricular anterior wall and a reduction ($P < 0.05$) in left ventricular internal diameter. Importantly, echocardiography also demonstrates increases ($P < 0.05$) in maximum and minimum left atrial area (Fig. 1B–D). These data demonstrate that Ang II treatment causes hypertension and ventricular hypertrophy as well as atrial enlargement.

Next, we used an intracardiac electrophysiology catheter to assess susceptibility to AF during burst pacing (Fig. 2A) in anesthetized mice treated with saline or Ang II. These studies show that 50% of Ang II treated mice were induced into AF compared to only 7% of saline treated mice (Fig. 2B). Furthermore, the duration of arrhythmia was very brief, lasting less that 5 s in the one saline treated mouse that was induced into AF. In contrast, 43% of Ang II treated mice induced into AF were in arrhythmia for > 5 s and 14% were in AF for longer than 30 s (Fig. 2C, Supplemental Table 2).

Additional assessment of atrial electrophysiology revealed that P wave duration (Fig. 2D) and atrial effective refractory period (AERP, Fig. 2E) were prolonged ($P < 0.05$) in Ang II treated mice. Furthermore, P-R interval and AV node effective refractory period (AVERP) were also increased ($P < 0.05$), while the P-R segment (measured from the end of the P wave to the start of the R wave) was not changed ($P = 0.86$), following Ang II treatment (Supplemental Table 3). These data demonstrate that Ang II treatment results in an increase in inducibility and severity of AF in association with impaired atrial conduction and altered atrial electrophysiology.

The prolongations in P wave duration and P-R interval were intrinsic to the atria and independent of the autonomic nervous system as illustrated in ECG recordings following autonomic nervous system blockade in intact anesthetized mice (Supplemental Fig. S2A). These studies demonstrate that autonomic blockade with an intraperitoneal injection of atropine and propranolol (10 mg/kg each) prolonged ($P < 0.05$) P wave duration (Supplemental Fig. S2B) and P-R interval (Supplemental Fig. S2C). Intrinsic P wave duration and P-R interval after blockade remained longer ($P < 0.05$) in Ang II treated mice compared to saline controls.

The effects of Ang II on atrial conduction and electrophysiology were further investigated using high resolution optical mapping in isolated atrial preparations. Representative activation maps (Fig. 3A) illustrate that conduction time across the atria is slower in Ang II treated hearts. Summary data show that cycle length in Ang II treated hearts is longer ($P < 0.05$) than in saline treated controls (Fig. 3B) and that right (Fig. 3C) and left (Fig. 3D) atrial conduction velocities are reduced ($P < 0.05$) following Ang II treatment. Since HR is reduced in Ang II treated mice in vivo and cycle length is prolonged in isolated atrial preparations, we also measured atrial conduction velocities in

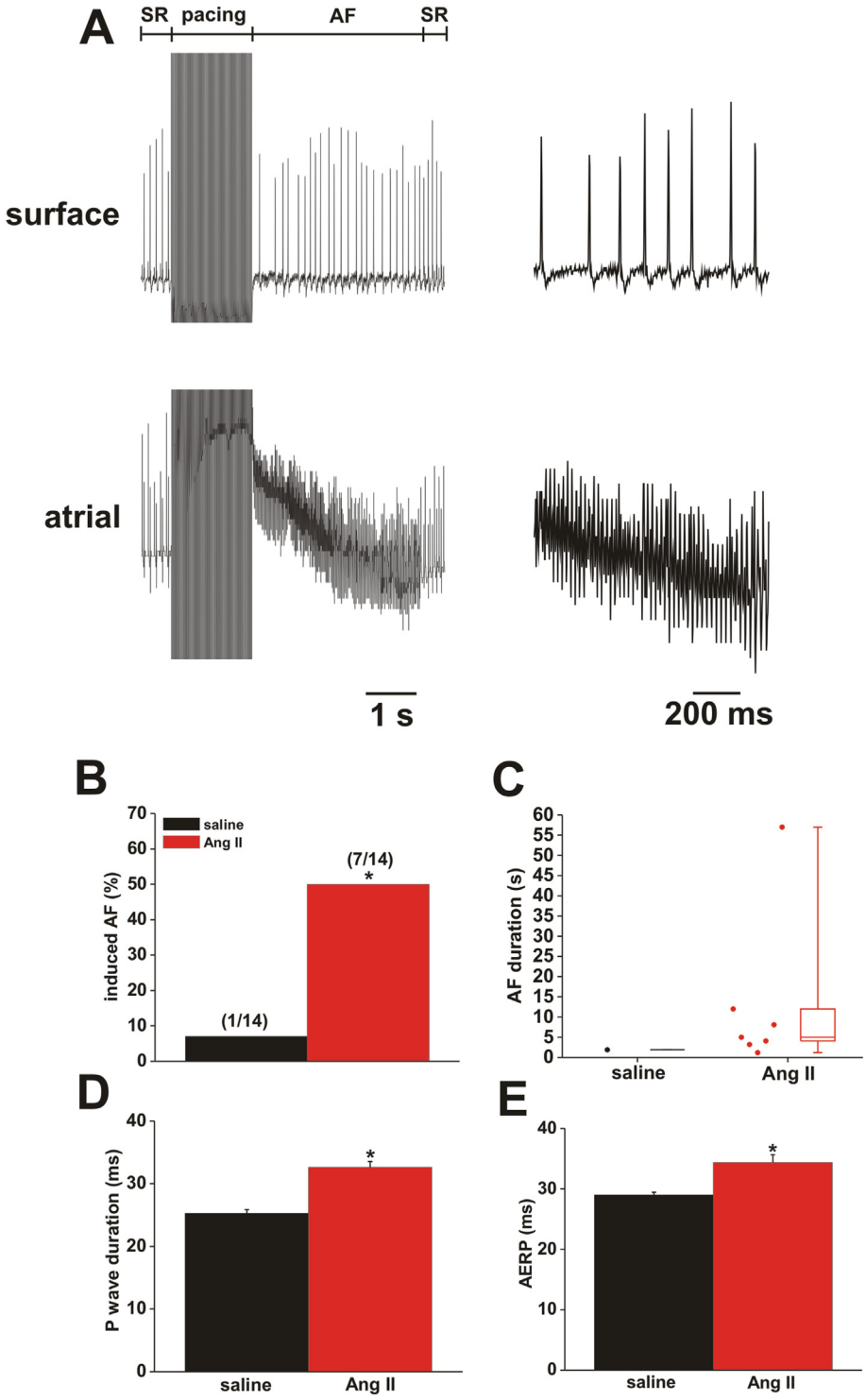

Fig. 2. Atrial fibrillation and atrial electrophysiology in Ang II treated mice. **A**, Representative surface (top) and intracardiac atrial (bottom) ECGs illustrating the induction of AF in an Ang II treated mouse following burst pacing in the right atrium. Recordings on the left illustrate the ECG during sinus rhythm (SR), the burst pacing period, the induction of AF, and the spontaneous reversion back to SR. Recordings on the right illustrate ECG patterns during AF. **B**, Summary of inducibility of AF in saline and Ang II treated mice. Numbers in parentheses indicate the number of mice induced into AF. $^{*}P = 0.03$ vs. saline by Fisher's exact test. **C**, Summary of the duration of AF in the saline and Ang II treated mice that were induced into AF. Refer to Supplemental Table 2 for additional AF analysis. **D**, Summary of P wave duration in mice treated with saline or Ang II. **E**, Summary of AERP in mice treated with saline or Ang II. For panels D and E $^{*}P < 0.05$ vs. saline by Student's *t*-test; $n = 15$ saline and 18 Ang II treated mice. Refer to Supplemental Table 3 for additional ECG and atrial electrophysiology analysis.

atrial preparations paced at a cycle length of 125 ms to account for rate dependent effects. These measurements confirm that right (Fig. 3E) and left (Fig. 3F) atrial conduction velocities are reduced ($P < 0.05$) following Ang II treatment independently of beating rate. Thus, our studies in vivo with and without autonomic nervous system blockade as well as optical mapping in atrial preparations confirm that atrial conduction is impaired by Ang II treatment.

We also measured right and left atrial AP duration in optical APs derived from our mapping studies (Fig. 3G). These data demonstrate that AP duration at 20% repolarization (APD_{20}; Fig. 3H) and 70% repolarization (APD_{70}, Fig. 3I) was prolonged ($P < 0.05$) in Ang II treated mice. Atrial AP morphology was further investigated in isolated myocytes as described below.

3.2. Effects of Ang II on atrial myocyte electrophysiology

To investigate the mechanisms for the effects of Ang II on AF inducibility and atrial electrophysiology, we measured AP morphology in right and left atrial myocytes isolated from saline or Ang II treated mice (Fig. 4A and B). Consistent with the hypertrophic response elicited by Ang II, left atrial myocytes displayed an increase ($P < 0.05$) in cell capacitance following Ang II treatment (Fig. 4C). On the other hand,

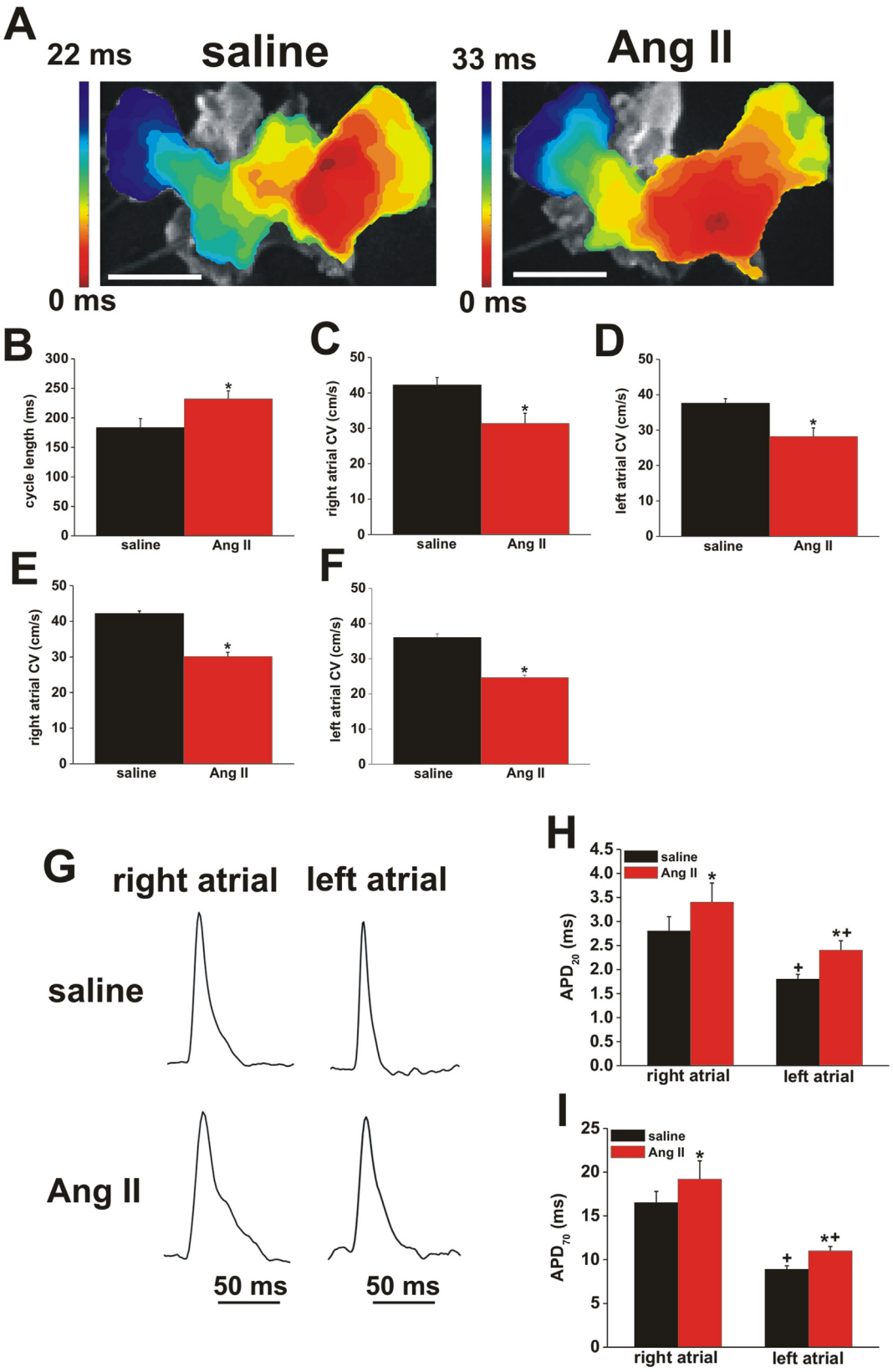

Fig. 3. Atrial electrical conduction properties in mice treated with Ang II. **A**, Representative activation maps in isolated atrial preparations from mice treated with saline or Ang II. The right atrial appendage is on the right side of the image. Red colour indicates the earliest activation time. Scale bars are 3 mm. **B**, Summary of cycle length in atrial preparations from saline and Ang II treated mice in sinus rhythm. **C and D**, right and left atrial conduction velocities in preparations from mice treated with saline or Ang II in sinus rhythm. **E and F**, right and left atrial conduction velocities in preparations paced at a cycle length of 125 ms. $^{*}P < 0.05$ vs. saline by Student's *t*-test; $n = 5$ atrial preparations per group. **G**, Representative right and left atrial optical APs from saline and Ang II treated mice. **H and I**, Summary data showing AP duration at 20% repolarization (APD_{20}, **H**) and 70% repolarization (APD_{70}, **I**). $^{*}P < 0.05$ vs. saline; $^{+}P < 0.05$ vs. right atrial by two-way ANOVA with Tukey's posthoc test; $n = 5$ per group. (For interpretation of the references to colour in this figure legend, the reader is referred to the web version of this article.)

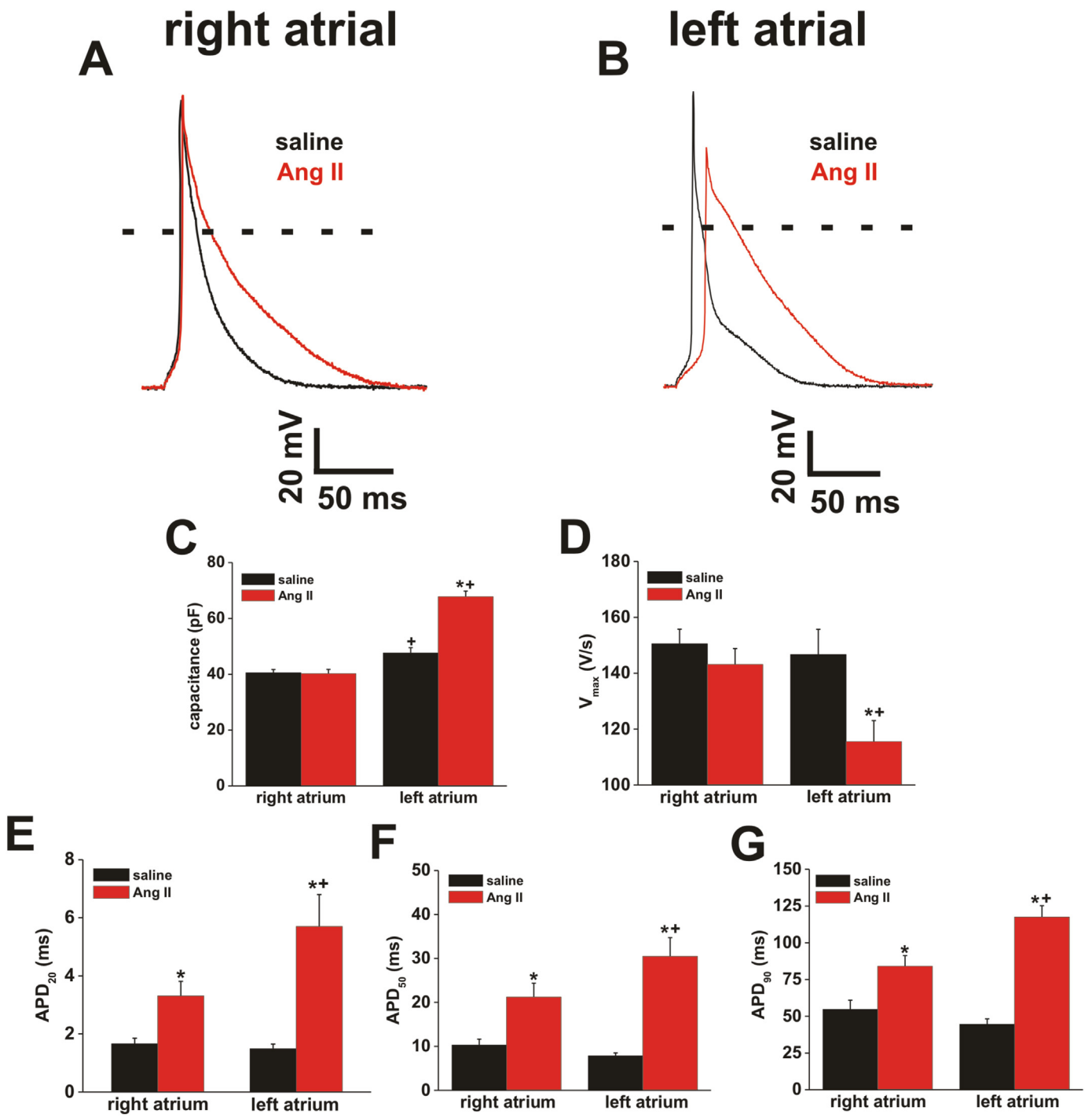

Fig. 4. Right and left atrial action potential morphology in mice treated with Ang II. **A and B**, Representative stimulated APs in isolated right (**A**) and left (**B**) atrial myocytes from mice treated with saline or Ang II. Cell capacitances for representative recordings are as follows. Right atrial/saline: 31.6 pF; right atrial/Ang II: 48.1 pF; left atrial/saline: 51.9 pF; left atrial/Ang II: 74.5 pF. **C**, Summary of cell capacitance in right and left atrial myocytes from saline or Ang II treated mice. **D**, Summary of AP V_{max} in right and left atrial myocytes from saline or Ang II treated mice. **E–G**, Summary of APD_{20} (**E**), APD_{50} (**F**) and APD_{90} (**G**) in right and left atrial myocytes from saline or Ang II treated mice. For all panels $^{*}P < 0.05$ vs. saline, $^{+}P < 0.05$ vs. right atrium by two-way ANOVA with Tukey's posthoc test, $n = 14$ saline and 12 Ang II treated myocytes for the right atrium, $n = 14$ saline and 15 Ang II treated myocytes for the left atrium. Refer to Supplemental Tables 4 and 5 for additional analysis of AP morphology.

there was no difference ($P = 0.90$) in capacitance in right atrial myocytes from saline and Ang II treated mice (Fig. 4C).

AP recordings revealed distinct patterns of electrical remodeling in right and left atrial myocytes following Ang II treatment. Specifically, Ang II had no effect on AP upstroke velocity (V_{max}; $P = 0.35$) or AP overshoot (OS; $P = 0.45$) in right atrial myocytes (Fig. 4D, Supplemental Table 4). In contrast, AP V_{max} ($P = 0.01$) and OS ($P = 0.004$) were reduced following Ang II treatment in left atrial myocytes (Fig. 4D, Supplemental Table 5). Furthermore, APD_{20} (Fig. 4E), APD_{50} (Fig. 4F) and APD_{90} (Fig. 4G) were increased ($P < 0.05$) in Ang II treated right and left atrial myocytes; however, these prolongations in APD were greater ($P < 0.05$) in left atrial myocytes (see also Supplemental Table 5).

To determine the basis for these changes in AP morphology, we

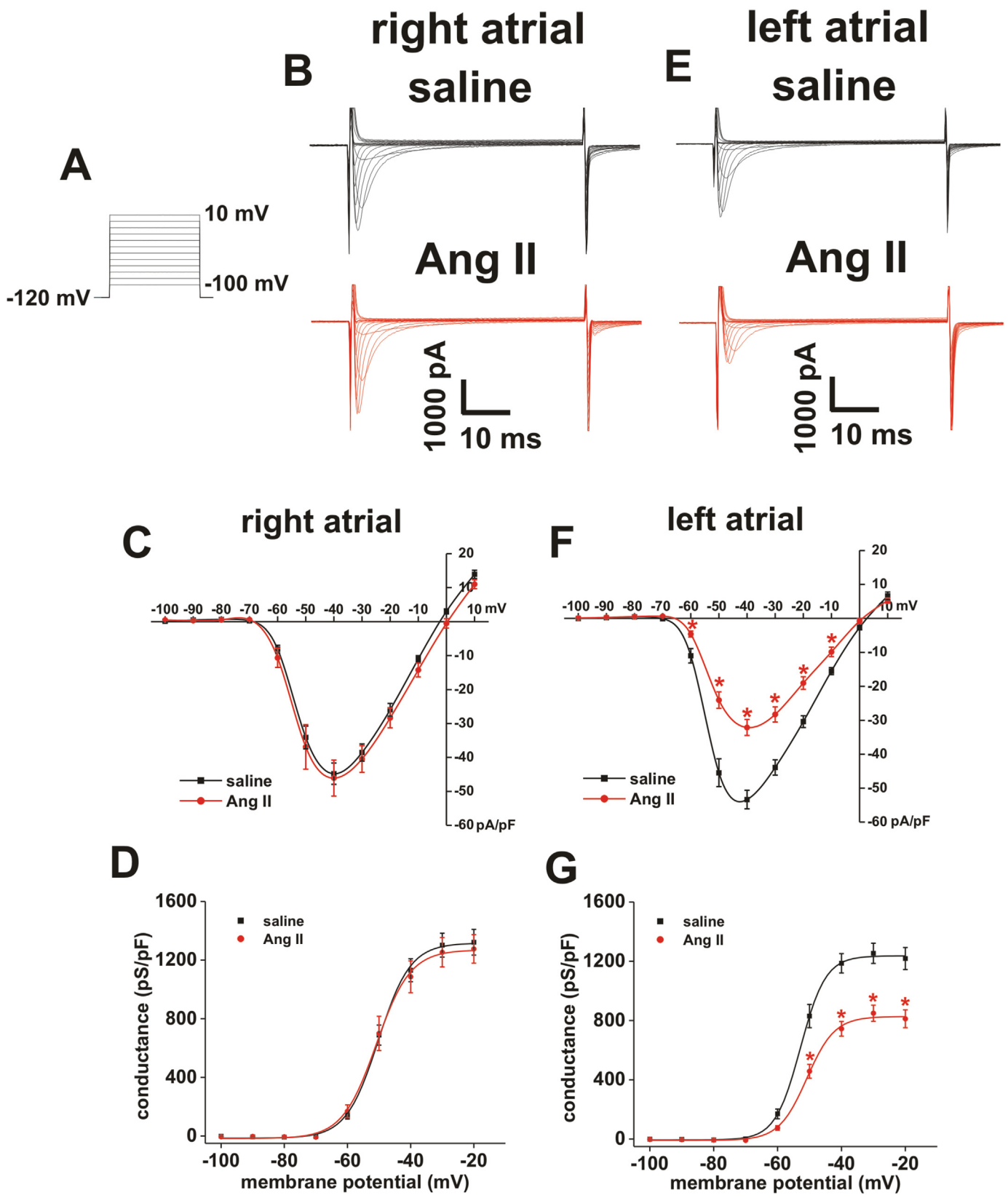

Fig. 5. Effects on Ang II treatment on atrial sodium current. **A**, Voltage clamp protocol used to measure I_{Na}. **B**, Representative I_{Na} recordings in right atrial myocytes from saline and Ang II treated mice. Cell capacitances for representative recordings are as follows. Right atrial/saline: 52 pF; right atrial/Ang II: 62 pF. **C**, I_{Na} IV curves in right atrial myocytes from saline and Ang II treated mice. **D**, Summary I_{Na} activation curves in right atrial myocytes from saline and Ang II treated mice. For panels C and D $n = 13$ saline and 12 Ang II treated right atrial myocytes. **E**, Representative I_{Na} recordings in left atrial myocytes from saline and Ang II treated mice. Cell capacitances for representative recordings are as follows, left atrial/saline: 33 pF; left atrial/Ang II: 57 pF. **F**, I_{Na} IV curves in left atrial myocytes from saline and Ang II treated mice. **G**, Summary I_{Na} activation curves in left atrial myocytes from saline and Ang II treated mice. For panels F and G $n = 17$ saline and 18 Ang II treated myocytes. $^*P < 0.05$ vs. saline at each membrane potential by two-way repeated measures ANOVA with Tukey's posthoc test. Refer to Supplemental Table 6 for a summary of I_{Na} activation kinetics.

measured I_{Na} under voltage clamp conditions (Fig. 5A) in right and left atrial myocytes from saline and Ang II treated mice. Consistent with the lack of a difference in right atrial V_{max}, I_{Na} in right atrial myocytes (Fig. 5B) was unaffected by Ang II. Specifically, IV curves demonstrate no differences ($P = 0.25$) in I_{Na} density (Fig. 5C) and activation curves show that conductance density was not affected ($P = 0.65$) by Ang II (Fig. 5D). Analysis of I_{Na} activation kinetics confirmed there were no differences in maximum conductance (G_{max}, $P = 0.22$) or the voltage for 50% channel activation ($V_{1/2(act)}$, $P = 0.30$) in Ang II treated right atrial myocytes (Supplemental Table 6). Conversely, Ang II treatment potently reduced I_{Na} in left atrial myocytes (Fig. 5E). IV analysis confirms that I_{Na} density (Fig. 5F) and I_{Na} conductance (Fig. 5G) were reduced ($P < 0.05$) in left atrial myocytes from Ang II treated mice. Furthermore, analysis of I_{Na} activation kinetics shows that G_{max} ($P < 0.001$) was reduced in association with a right shift ($P = 0.03$) in $V_{1/2(act)}$ (Supplemental Table 6). A reduction in left atrial I_{Na} is consistent with the reductions in left atrial AP V_{max} and OS.

Subsequently, we investigated the mechanisms for the selective reduction in left atrial I_{Na} following Ang II treatment. Na^+ channel function and biophysics are importantly regulated by protein kinase C (PKC) [23]. Furthermore, pathologically elevated Ang II has been shown to cause an increase in PKC activity [24]. Accordingly, we hypothesized that enhanced PKC activity may underlie the reduction in left atrial I_{Na} in Ang II treated mice. We first tested this by dialyzing left atrial myocytes from Ang II treated mice with the PKC inhibitor bisindolylmaleimide 1 [25] (BIM 1, 1 μM, Fig. 6A). For controls, I_{Na} measurements were made from Ang II treated myocytes not receiving BIM 1 from the same myocyte isolations as those used for BIM 1 studies. Summary IV curves illustrate that BIM 1 potently reversed ($P < 0.05$) the reduction in left atrial I_{Na} density (Fig. 6B) and increased ($P < 0.05$) I_{Na} conductance (Fig. 6C) compared to untreated (control) Ang II treated myocytes. Following BIM 1 application I_{Na} density (Fig. 6B, $P = 0.76$) and I_{Na} conductance (Fig. 6C, $P = 0.65$) were not different from saline controls. Analysis of I_{Na} activation kinetics demonstrates that BIM 1 application increased ($P < 0.001$) G_{max} and shifted ($P < 0.05$) the $V_{1/2(act)}$ to more negative membrane potentials (Supplemental Table 7). Following BIM 1 application, G_{max} ($P = 0.97$) and $V_{1/2(act)}$ ($P = 0.51$) were also not different from saline controls. BIM1 had no effect on I_{Na} in left atrial myocytes from saline treated mice (Supplemental Fig. S3A). Specifically, summary IV curves (Supplemental Fig. S3B) and activation curves (Supplemental Fig. S3C) show that BIM1 did not affect I_{Na} density ($P = 0.94$) or I_{Na} conductance ($P = 0.96$) in saline treated left atrial myocytes. Furthermore, analysis of I_{Na} activation kinetics demonstrates that BIM1 had no effects on G_{max} ($P = 0.81$) or $V_{1/2(act)}$ ($P = 0.78$) in saline treated mice (Supplemental Table 8).

Next we measured the expression of PKCα in the right and left atria from saline and Ang II treated mice using Western blotting (Fig. 6D). These studies demonstrate that Ang II treatment resulted in an increase ($P < 0.05$) in PKCα expression in the left atrium, but not in the right atrium ($P = 1.00$). The mRNA expression of SCN5a, the gene underlying $Na_V1.5$, was not affected ($P = 0.97$) by Ang II in right or left atria (Fig. 6E). Collectively, these data demonstrate that the Ang II mediated reduction in left atrial I_{Na} occurs in association with enhanced PKC activity specifically in the left atrium.

The next series of experiments investigated the ionic and molecular mechanisms underlying the Ang II mediated prolongation of the AP in right and left atrial myocytes. We first focused on repolarizing K^+ currents and measured I_K between −100 and + 80 mV using voltage clamp protocols with and without a pre-pulse to −40 mV to inactivate I_{to} [26,27] (Fig. 7A and B). Summary IV curves illustrate that peak I_K from recordings without the pre-pulse was reduced ($P < 0.05$) in Ang II treated right atrial myocytes (Fig. 7C). IV curves for peak I_K measured from recordings with an inactivating pre-pulse (Fig. 7D) demonstrate that I_K remains reduced ($P < 0.05$) in Ang II treated right atrial myocytes, although to a smaller extent than that seen in recordings without the pre-pulse. Accordingly, IV relationships for the difference current between protocols with and without the inactivating pre-pulse, which is a representation of I_{to}, show that I_{to} is reduced ($P < 0.05$) in right atrial myocytes from Ang II treated mice (Fig. 7E). This is clearly evident in the representative I_K recordings without the pre-pulse, which show a pronounced reduction in early peak outward I_K in Ang II treated myocytes.

I_K was also investigated in left atrial myocytes from saline and Ang II treated mice using the same voltage clamp protocols (Fig. 7B). The representative recordings again show that the early peak outward I_K in recordings without a pre-pulse are largely absent in Ang II treated left atrial myocytes. Summary I_K IV curves for recordings without the pre-pulse (Fig. 7F) and with the pre-pulse (Fig. 7G) show that repolarizing I_K is reduced ($P < 0.05$) in Ang II treated left atrial myocytes. Furthermore, I_{to}, measured as the difference current between protocols, was reduced ($P < 0.05$) in left atrial myocytes from Ang II treated mice (Fig. 7H).

The degree of reduction in I_{to} elicited by Ang II was directly compared in right and left atrial myocytes (Supplemental Fig. S4A). Summary data illustrate that the reduction in I_{to} density (measured at +50 mV) was greater ($P < 0.05$) in left atrial myocytes compared to right atrial myocytes (Supplemental Fig. S4B). A larger reduction in I_{to} in left atrial myocytes is consistent with the greater increase in AP duration in left atrial myocytes from Ang II treated mice.

I_{to} activation kinetics were assessed by fitting a Boltzmann function to measurements of I_{to} conductance derived from the data in Fig. 7E and H. These data (Supplemental Fig. S4C–H) demonstrate that Ang II causes a right shift ($P < 0.05$) in the I_{to} activation curve in right and left atrial myocytes. Consistent with this, the voltage at which 50% of channels are activated ($V_{1/2(act)}$) was shifted ($P < 0.05$) to more positive values in right (Supplemental Fig. S4D) and left (Supplemental Fig. S4G) atrial myocytes. Consistent with the greater reduction in I_{to} in the left atrium, the I_{to} $V_{1/2(act)}$ in Ang II treated left atrial myocytes (35.2 ± 2.3 mV) was more positive ($P < 0.05$) than in Ang II treated right atrial myocytes (15.7 ± 7.4 mV).

Next, we measured the mRNA and protein expression of key I_{to} related genes, including KCND2 and KCND3 (underlie $K_V4.2$ and $K_V4.3$) as well as KCNIP2 (underlies the β subunit KChIP2) [28]. The mRNA expression of KCND2, KCND3 and KCNIP2 was assessed in the right and left atria from saline and Ang II treated mice (Supplemental Fig. S5A–C). KCND2, KCND3, and KCNIP2 were each reduced ($P < 0.05$) in the left atrium in Ang II treated mice. On the other hand, expression of these genes was not altered in the right atrium following Ang II treatment. Western blotting experiments demonstrate that, despite some alterations in mRNA expression, there was no difference in the protein expression of $K_V4.2$, $K_V4.3$ or KChIP2 in the right or left atria following Ang II treatment (Supplemental Fig. S5D–F).

In addition to I_{to}, repolarization in the atria is importantly affected by an ultrarapid delayed rectifier K^+ current (I_{Kur}) mediated by $K_V1.5$ channels. I_{Kur} can be measured as the component of repolarizing K^+ current sensitive to 4-aminopyridine (4-AP; 100 μM) [26,29]. We measured 4-AP sensitive I_{Kur} in right and left atrial myocytes from saline and Ang II treated mice (Supplemental Fig. S6A). Summary data demonstrate that 4-AP sensitive I_K was larger ($P < 0.05$) in saline treated left atrial myocytes and reduced ($P < 0.05$) to similar levels in both right and left atrial myocytes after Ang II treatment (Supplemental Fig. S6B). This indicates that I_{Kur} is reduced in both atria by Ang II. The mRNA expression of KCNA5 (underlies $K_V1.5$) was not altered ($P = 0.348$) by Ang II in the right atrium and was increased ($P < 0.05$) by Ang II in the left atrium (Supplemental Fig. S6C). Nevertheless, Western blotting (Supplemental Fig. S6D) demonstrates that Ang II had no effects on expression of $K_V1.5$ protein in the right atrium ($P = 0.38$) or left atrium ($P = 0.60$).

L-type Ca^{2+} channels also play a role in determining AP duration. Accordingly, we measured $I_{Ca,L}$ in right and left atrial myocytes from saline and Ang II treated mice (Supplemental Figs. S7A and S7B).

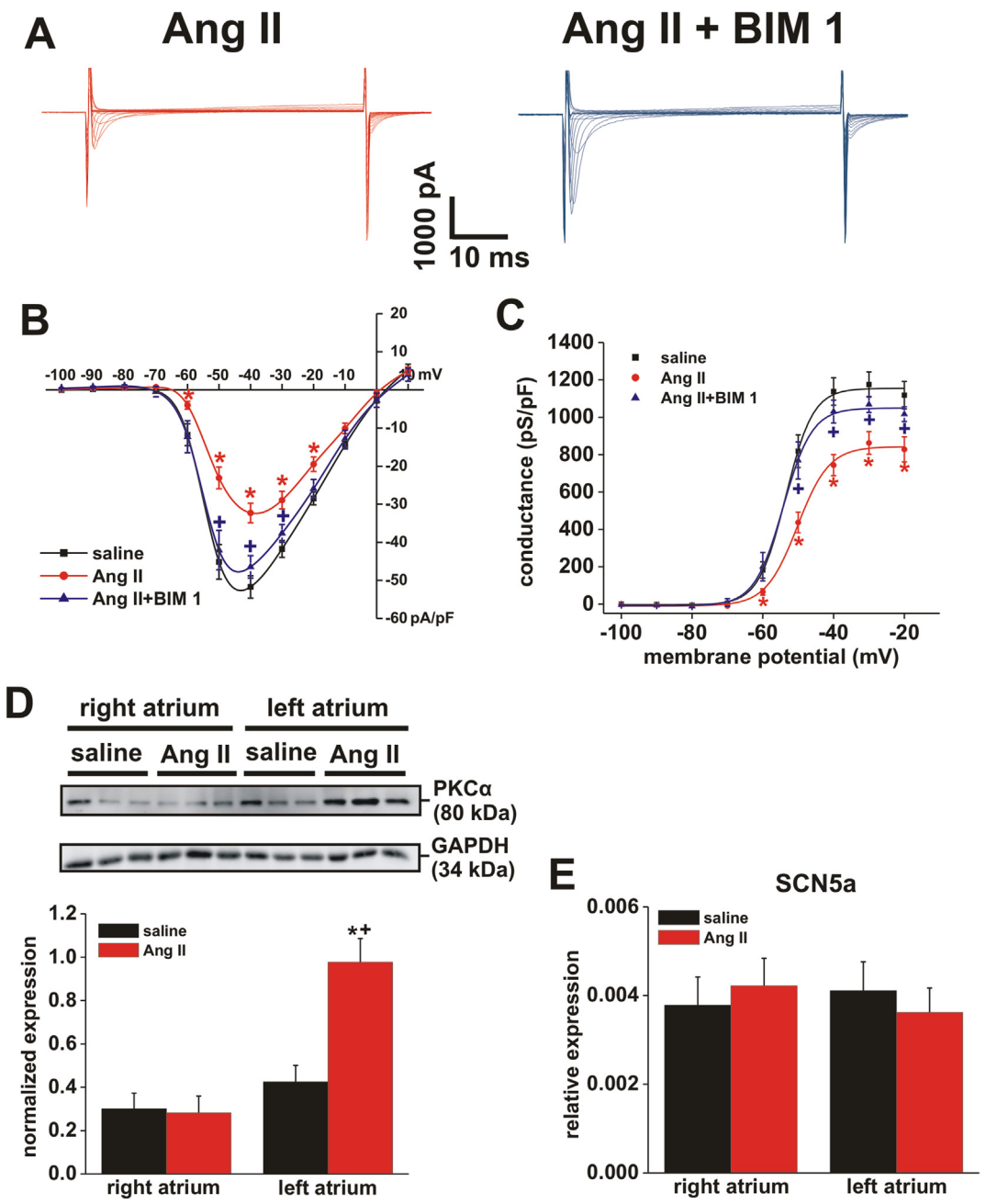

Fig. 6. Effects of protein kinase C inhibition on I_{Na} in Ang II treated mice. **A**, Representative I_{Na} recordings in Ang II treated left atrial myocytes following dialysis with the PKC inhibitor BIM 1 (1 μM) and in control myocytes. Cell capacitances for representative recordings are as follows. Ang II: 40 pF; Ang II + BIM 1: 50 pF. BIM 1 was dialyzed into the myocytes via the patch-clamp pipette for 5 min before recording. Voltage clamp protocol is as shown in Fig. 5A. **B**, Summary left atrial I_{Na} IV curves for saline, Ang II and Ang II with BIM 1 dialysis. **C**, Summary left atrial I_{Na} activation curves for saline, Ang II and Ang II with BIM 1 dialysis. For panels B and C $^{*}P < 0.05$ vs. saline, $^{+}P < 0.05$ vs. Ang II at each membrane potential by two-way repeated measures ANOVA with Tukey's posthoc test, $n = 12$ saline, 14 Ang II and 10 Ang II + BIM 1 left atrial myocytes. Refer to Supplemental Table 7 for a summary of I_{Na} activation kinetics. **D**, Expression of PKCα protein in the right and left atria from saline and Ang II treated mice. $^{*}P < 0.05$ vs. saline, $^{+}P < 0.05$ vs. right atrium by two-way ANOVA with Tukey's posthoc test; $n = 6$ atria per group. **E**, mRNA expression of SCN5a in the right and left atria of saline and Ang II treated mice. Ang II had no effect ($P = 0.97$) on expression of SCN5a in the right or left atria. Data analyzed by two-way ANOVA with Tukey's posthoc test, $n = 7$–8 atria per group.

Summary IV curves demonstrate that $I_{Ca,L}$ density was not affected in right ($P = 0.53$, Supplemental Fig. S7C) or left ($P = 0.80$, Supplemental Fig. S7D) atrial myocytes from Ang II treated mice. Similarly, Ang II treatment had no effects on $I_{Ca,L}$ conductance in right ($P = 0.52$, Supplemental Fig. S7E) or left ($P = 0.78$, Supplemental Fig. S7F) atrial myocytes. Analysis of activation kinetics further confirms that Ang II had no effect on atrial $I_{Ca,L}$ (Supplemental Table 9).

3.3. Effects of Ang II on atrial fibrosis

Structural remodeling was investigated by measuring interstitial atrial fibrosis using picrosirius red staining in the right and left atria in saline and Ang II treated mice (Fig. 8A). Summary data demonstrate that Ang II treatment increased ($P < 0.05$) atrial fibrosis similarly in the right and left atria (Fig. 8B). Collagen content in the atria was further quantified using hydroxyproline assays in the right and left atria. Collagen content was increased ($P < 0.05$) in both atria of Ang II

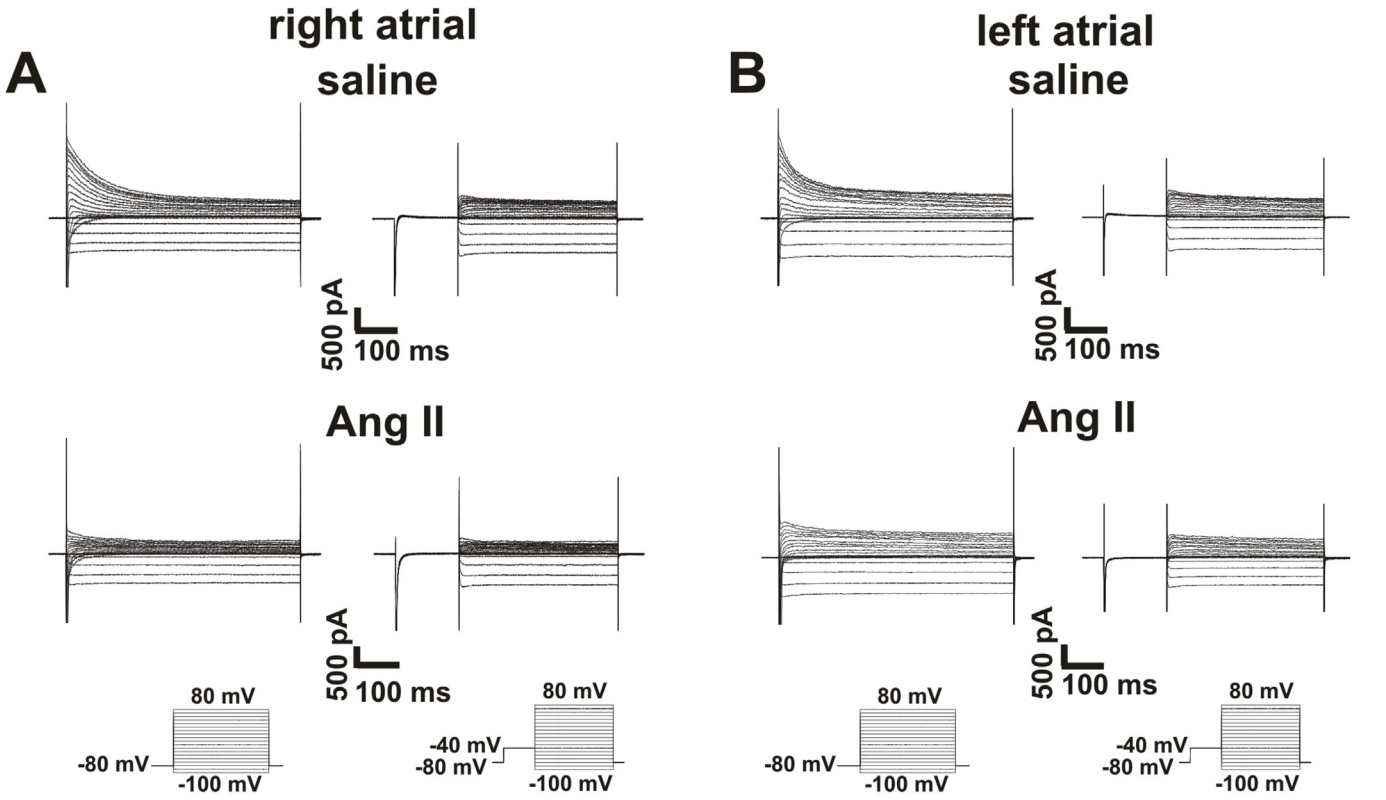

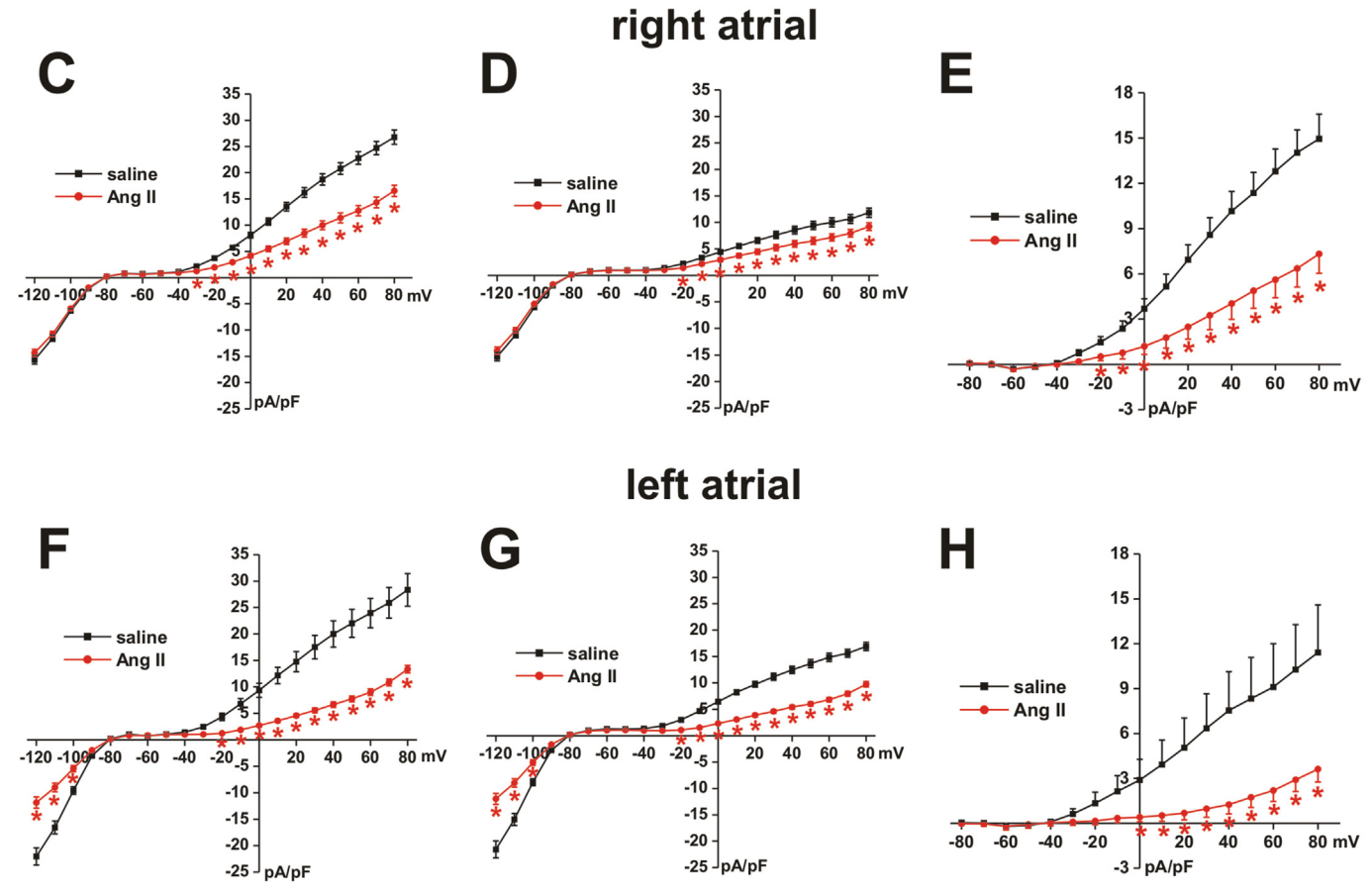

(caption on next page)

Fig. 7. Effects of Ang II on atrial potassium currents. **A and B**, Representative K^+ current recordings in right (**A**) and left (**B**) atrial myocytes from saline and Ang II treated mice. Currents were recorded with and without a pre-pulse to −40 mV to inactivate I_{to} as shown in the voltage clamp protocols at bottom of panels A and B. Cell capacitances for representative recordings are as follows. Right atrial/saline: 37.1 pF; right atrial/Ang II: 40 pF; left atrial/saline: 46.5; left atrial/Ang II: 63.5 pF. **C**, Summary right atrial I_K IV curves measured at the peak of the I_K recordings without the pre-pulse (recordings on the left in panel A). **D**, Summary right atrial I_K IV curves measured at the peak of the I_K recordings with the pre-pulse (recordings on the right in panel A). **E**, Summary right atrial I_K IV curves for the difference current between C and D, which is a measure of I_{to}. For panels C-E $^*P < 0.001$ vs. saline at each membrane potential by two-way repeated measures ANOVA with Tukey's posthoc test, $n = 17$ saline and 19 Ang II treated right atrial myocytes. **F**, Summary left atrial I_K IV curves measured at the peak of the I_K recordings without the pre-pulse (recordings on the left in panel B). **G**, Summary left atrial I_K IV curves measured at the peak of the I_K recordings with the pre-pulse (recordings on the right in panel B). **H**, Summary left atrial I_K IV curves for the difference current between F and G, which is a measure of I_{to}. For panels F–H $^*P < 0.001$ vs. saline at each membrane potential by two-way repeated measures ANOVA with Tukey's posthoc test, $n = 10$ saline and 17 Ang II treated left atrial myocytes.

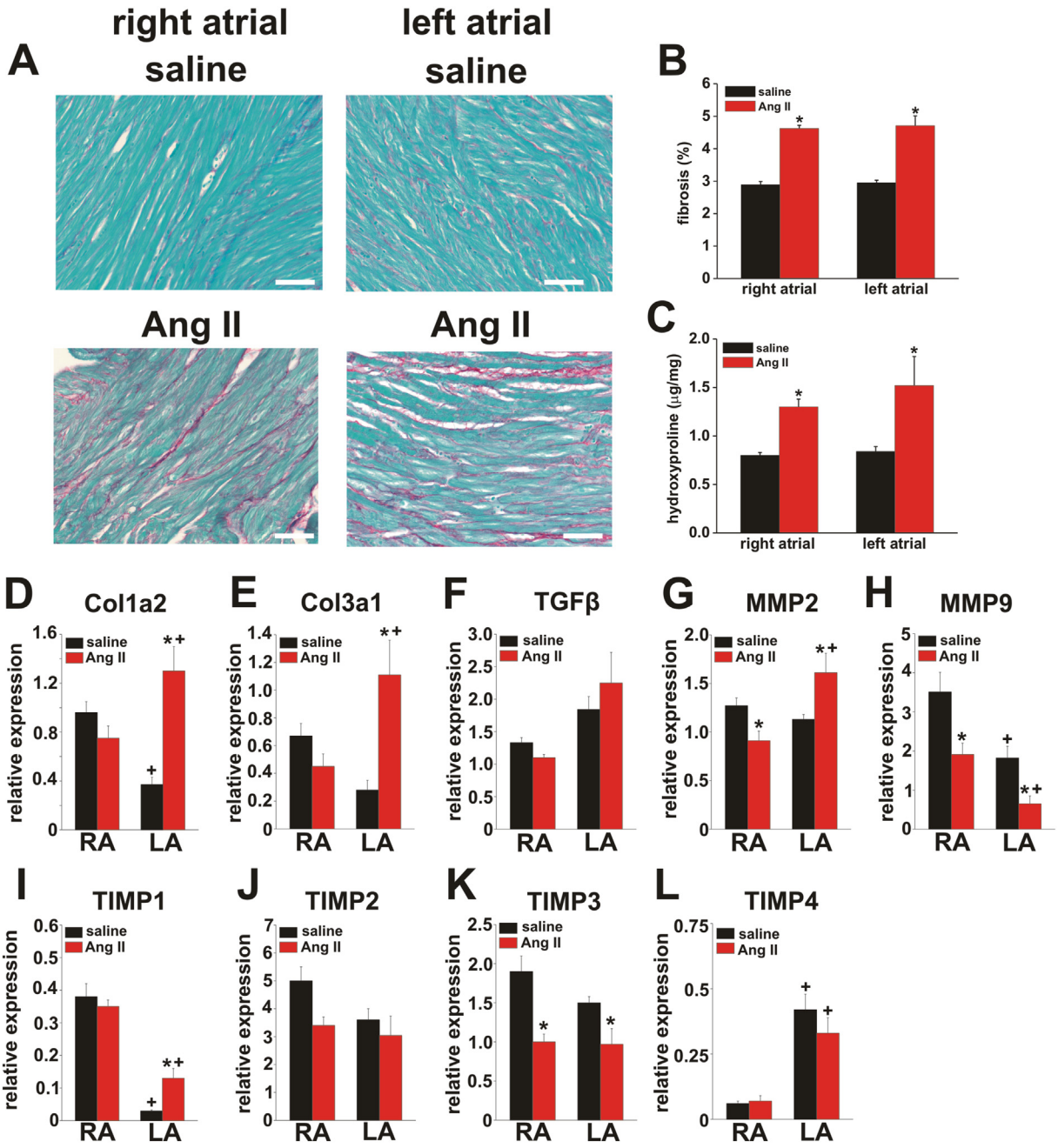

Fig. 8. Effects of Ang II on interstitial fibrosis in the atria. **A**, Representative images demonstrating patterns of interstitial fibrosis by picrosirius red staining (collagen fibres stained red) in the right and left atria from saline and Ang II treated mice. **B**, Summary of interstitial fibrosis in the right and left atria from saline and Ang II treated mice. $^*P < 0.001$ vs. saline by two-way ANOVA with Tukey's posthoc test, $n = 6$ atria per group. **C**, Summary of total collagen content in the right and left atria from saline and Ang II treated mice by hydroxyproline assay. $^*P = 0.005$ vs. saline by Student's *t*-test. There were no differences ($P = 0.44$) in collagen content between right and left atria. $n = 6$–7 samples for each group. **D–L**, Summary of the mRNA expression of collagen I (**D**), collagen III (**E**), TGFβ (**F**), MMP2 (**G**), MMP9 (**H**), TIMP1 (**I**), TIMP2 (**J**), TIMP3 (**K**) and TIMP4 (**L**) in the right (RA) and left (LA) atria in saline and Ang II treated mice. $^*P < 0.001$ vs. saline; $^+P < 0.05$ vs. right atrium by two-way ANOVA with Tukey's posthoc test, $n = 6$–8 samples per group. (For interpretation of the references to colour in this figure legend, the reader is referred to the web version of this article.)

treated mice (Fig. 8C).

We also measured the expression of mRNAs for genes involved in collagen production and extracellular matrix regulation, including matrix metalloproteinases (MMPs) and their inhibitors (TIMPs). Measurements were made in the right and left atria from mice treated with saline or Ang II. First, we measured expression of collagen type I (Col1a2; Fig. 8D) and collagen type III (Col3a1; Fig. 8E), which are the major interstitial collagens in the myocardium [30,31]. While Col1a2 ($P = 0.29$) and Col3a1 ($P = 0.34$) expression were not affected by Ang II in the right atrium, these collagen mRNAs were increased ($P < 0.001$) in the left atrium following Ang II treatment. TGFβ (Fig. 8F) was not altered ($P = 0.52$) by Ang II in the right or left atria. Next, we measured expression of MMP2 and MMP9, which are gelatinases that degrade collagens [12]. MMP2 was reduced ($P < 0.05$) in right atrium, but increased ($P < 0.05$) in the left atrium following Ang II treatment (Fig. 8G). MMP9 was reduced ($P < 0.05$) in the right and left atria by Ang II treatment (Fig. 8H). Finally, we measured the expression of TIMPs 1–4. TIMP1 expression was unchanged ($P = 0.08$) in the right atrium, but elevated ($P < 0.05$) in the left atrium after Ang II treatment (Fig. 8I). TIMP2 expression was not affected ($P = 0.07$) by Ang II in the right or left atria (Fig. 8J). TIMP3 expression was reduced ($P < 0.05$) in the right and left atria after Ang II treatment. TIMP4 was not altered ($P = 0.36$) by Ang II in the right or left atria (Fig. 8L). These data suggest that Ang II induced atrial fibrosis involves changes in collagen gene expression and/or alterations in extracellular matrix remodeling by MMPs and TIMPs (see Discussion).

4. Discussion

Our study demonstrates that mice induced into hypertension in the setting of enhanced Ang II are highly susceptible to AF, which was longer lasting compared to saline treated controls. This is consistent with human data indicating that elevated Ang II is linked to AF [4,5] and that enhancing angiotensin converting enzyme 2 (ACE2) activity, which opposes the effects of Ang II [32], protects against atrial remodeling [33]. Our assessment of P wave duration and AERP in vivo, as well as atrial conduction by high resolution optical mapping, indicate substantial alterations in atrial electrophysiology in Ang II treated mice, which we investigated in detail. These studies demonstrate that Ang II causes distinct patterns of electrical and structural remodeling in the right and left atria and provide novel insight into the cellular and molecular mechanisms for these alterations, thereby advancing our understanding of the basis for increased susceptibility to AF in the presence of pathologically elevated Ang II signaling.

Ang II caused extensive electrical remodeling, in association with changes in atrial AP morphology. Importantly, the changes in AP morphology were distinct in the right and left atria. Specifically, in right atrial myocytes, the major effect of Ang II treatment was an increase in AP duration. Other measurements of AP morphology were unaltered. Furthermore, cell capacitance was not affected in right atrial myocytes from Ang II treated mice. In contrast, left atrial myocytes showed a much greater prolongation of the AP as well as a substantial reduction in V_{max} and OS. Left atrial myocytes also displayed increased capacitance indicating the development of hypertrophy in these cells. This is consistent with our echocardiography data illustrating an increase in left atrial area after Ang II treatment. Thus, our experiments revealed that Ang II induced electrical remodeling is substantially more extensive in the left atrium compared to the right, which was previously unknown.

The reduction in left atrial, but not right atrial V_{max} was associated with a reduction in I_{Na} specifically in the left atrium. This reduction in left atrial I_{Na} occurred in association with a right shift in the voltage dependence of channel activation, which was reversed by inhibiting PKC. This is consistent with previous studies that have shown that PKC can modulate I_{Na} in ventricular myocytes and in heterologous expression systems [23,24,34,35]. We confirmed that PKCα, in particular, was significantly elevated in the left atrium, but not the right atrium, from Ang II treated mice. The PKC inhibitor we used (BIM 1) is not selective for PKCα; therefore, we cannot rule out contributions from other PKC isoforms; however, the robust Ang II induced increase in expression of PKCα specifically in the left atrium suggests an important role for this PKC isoform. The mRNA expression of SCN5a was not affected by Ang II indicating that elevated PKC activity is a major mechanism by which Ang II affects atrial I_{Na}. The reduction in left atrial I_{Na} in Ang II treated mice could contribute to the slowing of atrial conduction, which would decrease the wavelength of re-entry and favor AF.

Our investigations into the basis for the prolongation of the AP in Ang II treated mice revealed that I_{to} is reduced in right and left atrial myocytes, with the reduction in the left atrium being significantly larger than in the right atrium. This reduction in I_{to} occurred in association with significant changes in activation kinetics, suggesting that Ang II treatment leads to alterations in biophysical properties of the channels ($K_V4.2$, $K_V4.3$) that underlie I_{to}. I_{Kur} (measured as 4-AP sensitive I_K) was also reduced in both atria. This suggests that I_{to} and I_{Kur} are critically involved in the delayed repolarization in the atria following Ang II treatment. Right and left atrial $I_{Ca,L}$, on the other hand, was not affected by Ang II treatment.

Interestingly, our study shows that genes related to I_{to}, including KCND2, KCND3 and KCNIP2, were reduced in the left atrium, but were unaltered in the right atrium after Ang II treatment. This prompted us to investigate the expression of $K_V4.2$, $K_V4.3$ and KChIP2 by Western blotting. Surprisingly, we found no differences in expression of these proteins that underlie I_{to} in either atria after Ang II treatment. Similarly, despite some changes in mRNA expression of KCNA5, Ang II had no effect on protein expression of $K_V1.5$. Thus, the Ang II induced reductions in atrial I_{to} and I_{Kur} are not explained by changes in overall channel expression. These data suggest that the change in activation kinetics is a major contributor to the Ang II mediated reduction in I_{to}. Consistent with this, the $V_{1/2(act)}$ in Ang II treated left atrial myocytes was more positive than in Ang II treated right atrial myocytes. Nevertheless, it is possible other factors also contribute to the changes in K^+ currents observed following Ang II treatment. For example, it is possible that Ang II may affect K^+ channel trafficking, thereby regulating the number of functional channels in the plasma membrane and that this could contribute to the reduction in atrial I_{to} and I_{Kur}. This hypothesis is based on studies demonstrating that Ang II can promote the internalization of Kv4.3 channels [36]. Similarly, prior studies have shown that Ang II promotes internalization of K^+ channels in other cell types [37]. Additional studies are required to determine whether the effects of Ang II on atrial I_{to} and I_{Kur} involve changes in channel trafficking. Atrial repolarization and I_K is also determined by $K_V2.1$ channels; however, the role of these channels was not investigated in the present study. A reduction in I_{to}/I_{Kur} and a prolongation of the atrial AP could increase the likelihood of EADs, which could contribute to the increased susceptibility to AF in Ang II mediated hypertension [38].

The observation that Ang II induced electrical remodeling was more extensive in the left atrium may have implications for understanding the increased susceptibility to AF in vivo. Although it can involve both atria, it is generally thought that AF is more commonly initiated in the left atrium [39–42]. This can involve the pulmonary vein-left atrial junction, but also other regions of the left atrium, including the left atrial appendage [39,41,43]. We observed more severe electrical remodeling in the left atrium, including a reduction in AP upstroke velocity and greater prolongation of AP duration, which may contribute substantially to the increased susceptibility to AF and is consistent with the left atrium playing a critical role in AF generation and maintenance observed clinically. Interestingly, a prior study in human patients with persistent AF demonstrated left-to-right differences in inward rectifier K^+ current [44] further supporting the idea that differential remodeling in the left and right atria is a factor in the development of AF. The basis for more severe electrical remodeling in left atrial myocytes is not known; however, it was notable that cell capacitance was increased

(indicating cellular hypertrophy) in left atrial, but not right atrial myocytes from Ang II treated mice. This suggests that, unlike the left atrium, the right atrium did not develop Ang II induced hypertrophy; however, as we did not assess right atrial size by echocardiography, additional studies will be needed to further assess this. Thus, our data suggest that overall disease development and/or progression is enhanced in the left atria. The basis for these regional differences warrants further study.

Our optical mapping studies demonstrated that conduction velocity was reduced in the right and left atrium following Ang II treatment; however, AP V_{max} and I_{Na} were reduced only in left atrial myocytes. This suggested that additional factors contribute to the slowing of atrial conduction. Accordingly, we also measured the effects of Ang II on atrial fibrosis and found that interstitial fibrosis and collagen content were increased in both the right and left atria. The increase in atrial fibrosis occurred in association with a number of gene expression changes. Notably, expression of collagen I and collagen III was increased in the left atrium, but not the right atrium. TGFβ, a well known driver of collagen gene expression and fibrosis [6,45] was not altered in either atria following Ang II treatment; however, TIMP1, which has recently been shown to contribute to Ang II mediated ventricular fibrosis by increasing collagen gene expression independent of effects on MMPs [46], was increased in the left atrium of Ang II treated mice. This suggests that TIMP1 may play a role in the increased collagen gene expression in the left atrium following Ang II treatment. We also observed reductions in TIMP3 in the right and left atria of Ang II treated mice. TIMP3 knockout mice have been shown to develop ventricular fibrosis due to post-translational stabilization and deposition of collagens by matricellular proteins [47]; thus, reductions in right and left atrial TIMP3 may be profibrotic in the atria through related mechanisms to those identified in the ventricles. Finally, we observed reductions in the expression of MMP2 in the right atrium as well as MMP9 in both atria. Reductions in MMPs could alter the balance between MMP and TIMP activity leading to impaired breakdown of collagens in the extracellular matrix and increased interstitial fibrosis [12,30]. Thus, our findings suggest that the increases in right and left atrial fibrosis in Ang II treated mice could occur due to a number of alterations, including increases in collagen gene expression as well as changes in the expression of MMPs and/or TIMPs. Additional studies will be needed to determine the specific mechanisms and relative importance of these different signaling molecules.

Determining the mechanisms that underlie Ang II mediated atrial fibrosis will be important as increases in atrial fibrosis would be expected to contribute to a slowing of conduction throughout the right and left atria in Ang II treated mice. When considered collectively, our findings suggest that the substrate for AF is created by both a reduction in atrial I_{Na} (particularly in the left atrium) and enhanced fibrosis throughout the atria (right and left). These alterations could combine to substantially slow electrical conduction in the atria and impair normal conduction patterns, thereby favoring the maintenance of AF.

Comparing our findings with other studies further supports the conclusion that Ang II mediated hypertension elicits distinct effects on atrial electrophysiology and arrhythmogenesis. For example, chronic Ang II treatment has been shown to reduce the expression of KCND2 and KCND3 in the left ventricle; however, KChIP2 was unaltered and I_{to} density was not affected [48]. Also, ventricular hypertrophy induced by transverse aortic constriction does cause a reduction in left ventricular I_{to} density; however, this occurred due to cardiomyocyte hypertrophy. Expression of KCND2, KCND3 and KChIP2 were unaffected in the left ventricle following aortic constriction [49]. In contrast to our findings with Ang II treatment, transverse aortic constriction did not alter the expression of KCND2 or KCND3 in the atria (unspecified region) [50]. Finally, transverse aortic constriction does cause atrial enlargement, but, in contrast to our findings in Ang II treatment, was not associated with increased atrial (unspecified region) fibrosis [50]. Thus, Ang II mediated hypertension distinctly reduces atrial, but not ventricular I_{to}, and promotes atrial fibrosis, by mechanisms that are distinct from those observed in other conditions associated with increased afterload and cardiac hypertrophy such as aortic constriction.

The effects of Ang II in the heart are complex and the basis for AF in Ang II mediated hypertension are likely to be multifactorial. Consistent with this, recent studies have shown that changes in the immunoproteasome and oxidative stress can each contribute to the increased susceptibility to AF during Ang II treatment [6,51]. One consequence of oxidative stress is the oxidation and pathological activation of Ca^{2+}/calmodulin-dependent protein kinase II (CaMKII), which has been linked to Ang II mediated AF [51]. Furthermore, CaMKII can modulate the activity of ion channels including Na^+ and K^+ channels [52]. Accordingly, it will be important to investigate the role of CaMKII (including phosphorylated or oxidized forms) in the context of our findings in future studies. It should also be noted that, while our Ang II treatment protocol led to hypertension and hypertrophy with fibrosis, mice did not develop systolic heart failure. Nevertheless, hypertrophy and fibrosis, if left uncorrected, can ultimately lead to heart failure, which itself is associated with the occurrence of AF [5]. Thus, the development and progression of AF in these settings can be complex. Our study addresses some of these issues and further enhances our understanding of Ang II mediated changes in the atria that lead to a substrate for AF and show that electrical and structural remodeling are prevalent in the atria following Ang II treatment. Our study identifies I_{Na}, I_{to}, and I_{Kur} as critical ion channels involved in electrical remodeling and also shows that atrial fibrosis develops in association with changes in expression of genes involved in collagen production and extracellular matrix regulation. We also identify PKCs (including PKCα) as a novel molecular target involved in Ang II mediated electrical remodeling in the left atrium. These may represent new therapeutic targets for the treatment of AF in Ang II mediated hypertension. As several of these proteins are also present in the ventricular myocardium, it may be important to consider approaches to modulate these targets selectively in the atria.

The mechanisms leading to AF in general are still incompletely understood, but are thought to involve triggered activity in the setting of a substrate that favours re-entry [5]. The likelihood of re-entry occurring is increased when the wavelength is reduced. As discussed above, several of the alterations we observed are consistent with this theory of arrhythmogenesis. The increases in AP duration in right and left atria of Ang II treated mice could lead to EADs, which can trigger AF [5]. Furthermore, increased fibrosis in both atria and reduced I_{Na} in the left atria can lead to slow conduction (as we observed), which can shorten the wavelength of re-entry [5]. On the other hand, longer APs, while favoring triggered activity, can also increase atrial refractoriness (observed in our in vivo studies), which could lessen the likelihood of re-entry. As we clearly observed increased susceptibility and severity of AF in Ang II treated mice, more work will be needed to determine the extent to which triggered activity and/or electrical re-entry underlie AF in this model.

In conclusion, this study demonstrates that Ang II mediated hypertension increases the incidence and severity of AF in association with distinct patterns of structural and electrical remodeling in the atria. Specifically, electrical remodeling was more severe and more complex in the left atrium compared to the right atrium. Structural remodeling due to increased atrial fibrosis was present throughout the right and left atria. Increases in AP duration in the right and left atria could increase the likelihood of triggered activity (EADs) that could initiate AF while impaired atrial I_{Na} and enhanced atrial fibrosis are consistent with the slowing of atrial conduction that could shorten the wavelength of re-entry and lead to the maintenance of a substrate for AF. Our study identifies novel molecular changes that underlie these alterations. Additional experiments will help determine which of these could be used therapeutically to treat AF in Ang II mediated hypertension.

Conflicts of interest

None.

Acknowledgements

This work was supported by operating grants from the Canadian Institutes of Health Research to R.A.R (MOP 93718, 142486). R.A.R. holds a New Investigator Award from the Heart and Stroke Foundation of Canada. H.J.J. is the recipient of a Killam Postdoctoral Fellowship. M. M. is the recipient of a Libin Cardiovascular Institute of Alberta Graduate Scholarship. E.E.E. held a Heart and Stroke Foundation of Canada Fellowship.

Appendix A. Supplementary data

Supplementary data to this article can be found online at https://doi.org/10.1016/j.yjmcc.2018.09.011.

References

[1] U. Schotten, S. Verheule, P. Kirchhof, A. Goette, Pathophysiological mechanisms of atrial fibrillation: a translational appraisal, Physiol. Rev. 91 (2011) 265–325.
[2] M.J. Bloch, Worldwide prevalence of hypertension exceeds 1.3 billion, J. Am. Soc. Hypertens. 10 (2016) 753–754.
[3] K.T. Mills, J.D. Bundy, T.N. Kelly, J.E. Reed, P.M. Kearney, K. Reynolds, et al., Global disparities of hypertension prevalence and control: a systematic analysis of population-based studies from 90 countries, Circulation 134 (2016) 441–450.
[4] R. Khatib, P. Joseph, M. Briel, S. Yusuf, J. Healey, Blockade of the renin-angiotensin-aldosterone system (RAAS) for primary prevention of non-valvular atrial fibrillation: a systematic review and meta analysis of randomized controlled trials, Int. J. Cardiol. 165 (2013) 17–24.
[5] J. Heijman, N. Voigt, S. Nattel, D. Dobrev, Cellular and molecular electrophysiology of atrial fibrillation initiation, maintenance, and progression, Circ. Res. 114 (2014) 1483–1499.
[6] J. Li, S. Wang, J. Bai, X.L. Yang, Y.L. Zhang, Y.L. Che, et al., Novel role for the immunoproteasome subunit PSMB10 in Angiotensin II-induced atrial fibrillation in mice, Hypertension 71 (2018) 866–876.
[7] A. Fukui, N. Takahashi, C. Nakada, T. Masaki, O. Kume, T. Shinohara, et al., Role of leptin signaling in the pathogenesis of angiotensin II-mediated atrial fibrosis and fibrillation, Circ Arrhythm. Electrophysiol. 6 (2013) 402–409.
[8] S. Nattel, B. Burstein, D. Dobrev, Atrial remodeling and atrial fibrillation: mechanisms and implications, Circ Arrhythm. Electrophysiol. 1 (2008) 62–73.
[9] A.O. Grant, Cardiac ion channels, Circ Arrhythm. Electrophysiol. 2 (2009) 185–194.
[10] A.G. Kleber, Y. Rudy, Basic mechanisms of cardiac impulse propagation and associated arrhythmias, Physiol. Rev. 84 (2004) 431–488.
[11] J.M. Nerbonne, R.S. Kass, Molecular physiology of cardiac repolarization, Physiol. Rev. 85 (2005) 1205–1253.
[12] A. Takawale, S.S. Sakamuri, Z. Kassiri, Extracellular matrix communication and turnover in cardiac physiology and pathology, Compr. Physiol. 5 (2015) 687–719.
[13] M. Miragoli, A.V. Glukhov, Atrial fibrillation and fibrosis: beyond the cardiomyocyte centric view, Biomed. Res. Int. 2015 (2015) 798768.
[14] E.E. Egom, K. Vella, R. Hua, H.J. Jansen, M. Moghtadaei, I. Polina, et al., Impaired sinoatrial node function and increased susceptibility to atrial fibrillation in mice lacking natriuretic peptide receptor C, J. Physiol. 593 (2015) 1127–1146.
[15] H.J. Jansen, M. Moghtadaei, M. Mackasey, S.A. Rafferty, O. Bogachev, J.L. Sapp, et al., Atrial structure, function and arrhythmogenesis in aged and frail mice, Sci. Rep. 7 (2017) 44336.
[16] J.M. Tuomi, P. Chidiac, D.L. Jones, Evidence for enhanced M3 muscarinic receptor function and sensitivity to atrial arrhythmia in the RGS2-deficient mouse, Am. J. Physiol. Heart Circ. Physiol. 298 (2010) H554–H561.
[17] J. Azer, R. Hua, P.S. Krishnaswamy, R.A. Rose, Effects of natriuretic peptides on electrical conduction in the sinoatrial node and atrial myocardium of the heart, J. Physiol. 592 (2014) 1025–1045.
[18] P.S. Krishnaswamy, E.E. Egom, M. Moghtadaei, H.J. Jansen, J. Azer, O. Bogachev, et al., Altered parasympathetic nervous system regulation of the sinoatrial node in Akita diabetic mice, J. Mol. Cell. Cardiol. 82 (2015) 125–135.
[19] M. Moghtadaei, H.J. Jansen, M. Mackasey, S.A. Rafferty, O. Bogachev, J.L. Sapp, et al., The impacts of age and frailty on heart rate and sinoatrial node function, J. Physiol. 594 (2016) 7105–7126.
[20] V.V. Fedorov, I.T. Lozinsky, E.A. Sosunov, E.P. Anyukhovsky, M.R. Rosen, C.W. Balke, et al., Application of blebbistatin as an excitation-contraction uncoupler for electrophysiologic study of rat and rabbit hearts, Heart Rhythm. 4 (2007) 619–626.
[21] R. Hua, S.L. MacLeod, I. Polina, M. Moghtadaei, H.J. Jansen, O. Bogachev, et al., Effects of wild-type and mutant forms of atrial natriuretic peptide on atrial electrophysiology and arrhythmogenesis, Circ Arrhythm. Electrophysiol. 8 (2015) 1240–1254.
[22] J. Springer, J. Azer, R. Hua, C. Robbins, A. Adamczyk, S. McBoyle, et al., The natriuretic peptides BNP and CNP increase heart rate and electrical conduction by stimulating ionic currents in the sinoatrial node and atrial myocardium following activation of guanylyl cyclase-linked natriuretic peptide receptors, J. Mol. Cell. Cardiol. 52 (2012) 1122–1134.
[23] C. Marionneau, H. Abriel, Regulation of the cardiac Na+ channel NaV1.5 by post-translational modifications, J. Mol. Cell. Cardiol. 82 (2015) 36–47.
[24] S. Mathieu, N. El Khoury, K. Rivard, R. Gelinas, P. Goyette, P. Paradis, et al., Reduction in Na(+) current by angiotensin II is mediated by PKCalpha in mouse and human-induced pluripotent stem cell-derived cardiomyocytes, Heart Rhythm. 13 (2016) 1346–1354.
[25] D. Toullec, P. Pianetti, H. Coste, P. Bellevergue, T. Grand-Perret, M. Ajakane, et al., The bisindolylmaleimide GF 109203X is a potent and selective inhibitor of protein kinase C, J. Biol. Chem. 266 (1991) 15771–15781.
[26] A.E. Lomax, C.S. Kondo, W.R. Giles, Comparison of time- and voltage-dependent K+ currents in myocytes from left and right atria of adult mice, Am. J. Physiol. Heart Circ. Physiol. 285 (2003) H1837–H1848.
[27] H.C. Kuo, C.F. Cheng, R.B. Clark, J.J. Lin, J.L. Lin, M. Hoshijima, et al., A defect in the Kv channel-interacting protein 2 (KChIP2) gene leads to a complete loss of I(to) and confers susceptibility to ventricular tachycardia, Cell 107 (2001) 801–813.
[28] S. Grubb, K. Calloe, M.B. Thomsen, Impact of KChIP2 on cardiac electrophysiology and the progression of heart failure, Front. Physiol. 3 (2012) 118.
[29] C. Fiset, R.B. Clark, T.S. Larsen, W.R. Giles, A rapidly activating sustained K+ current modulates repolarization and excitation-contraction coupling in adult mouse ventricle, J. Physiol. 504 (1997) 557–563 Pt 3.
[30] Z. Kassiri, R. Khokha, Myocardial extra-cellular matrix and its regulation by metallo-proteinases and their inhibitors, Thromb. Haemost. 93 (2005) 212–219.
[31] D. Fan, A. Takawale, J. Lee, Z. Kassiri, Cardiac fibroblasts, fibrosis and extracellular matrix remodeling in heart disease, Fibrogenesis Tissue Repair 5 (2012) 15.
[32] V.B. Patel, J.C. Zhong, M.B. Grant, G.Y. Oudit, Role of the ACE2/Angiotensin 1-7 axis of the renin-angiotensin system in heart failure, Circ. Res. 118 (2016) 1313–1326.
[33] T. Zhou, Z. Wang, J. Fan, S. Chen, Z. Tan, H. Yang, et al., Angiotensin-converting enzyme-2 overexpression improves atrial remodeling and function in a canine model of atrial fibrillation, J. Am. Heart Assoc. 4 (2015) e001530.
[34] M. Liu, S. Sanyal, G. Gao, I.S. Gurung, X. Zhu, G. Gaconnet, et al., Cardiac Na+ current regulation by pyridine nucleotides, Circ. Res. 105 (2009) 737–745.
[35] W. Schreibmayer, N. Dascal, I. Lotan, M. Wallner, L. Weigl, Molecular mechanism of protein kinase C modulation of sodium channel alpha-subunits expressed in Xenopus oocytes, FEBS Lett. 291 (1991) 341–344.
[36] S.V. Doronin, I.A. Potapova, Z. Lu, I.S. Cohen, Angiotensin receptor type 1 forms a complex with the transient outward potassium channel Kv4.3 and regulates its gating properties and intracellular localization, J. Biol. Chem. 279 (2004) 48231–48237.
[37] M.D. Leo, S. Bulley, J.P. Bannister, K.P. Kuruvilla, D. Narayanan, J.H. Jaggar, Angiotensin II stimulates internalization and degradation of arterial myocyte plasma membrane BK channels to induce vasoconstriction, Am. J. Phys. Cell Phys. 309 (2015) C392–C402.
[38] S. Pepe, L.M. Delbridge, Pacemaker cell and atrial function: unravelling how calcium initiates and regulates the heart beat and how ionic dysfunction, 'channelopathies' and other membrane remodelling contribute to atrial fibrillation, Heart Lung Circ. 16 (2007) 331–334.
[39] Y.H. Yeh, C.T. Kuo, Y.S. Lee, Y.M. Lin, S. Nattel, F.C. Tsai, et al., Region-specific gene expression profiles in the left atria of patients with valvular atrial fibrillation, Heart Rhythm. 10 (2013) 383–391.
[40] P. Santangeli, E.S. Zado, M.D. Hutchinson, M.P. Riley, D. Lin, D.S. Frankel, et al., Prevalence and distribution of focal triggers in persistent and long-standing persistent atrial fibrillation, Heart Rhythm. 13 (2016) 374–382.
[41] P. Santangeli, F.E. Marchlinski, Techniques for the provocation, localization, and ablation of non-pulmonary vein triggers for atrial fibrillation, Heart Rhythm. 14 (2017) 1087–1096.
[42] M. Haissaguerre, M. Wright, M. Hocini, P. Jais, The substrate maintaining persistent atrial fibrillation, Circ Arrhythm. Electrophysiol. 1 (2008) 2–5.
[43] L. Di Biase, J.D. Burkhardt, P. Mohanty, J. Sanchez, S. Mohanty, R. Horton, et al., Left atrial appendage: an underrecognized trigger site of atrial fibrillation, Circulation 122 (2010) 109–118.
[44] N. Voigt, A. Trausch, M. Knaut, K. Matschke, A. Varro, D.R. Van Wagoner, et al., Left-to-right atrial inward rectifier potassium current gradients in patients with paroxysmal versus chronic atrial fibrillation, Circ Arrhythm. Electrophysiol. 3 (2010) 472–480.
[45] A. Leask, Getting to the heart of the matter: new insights into cardiac fibrosis, Circ. Res. 116 (2015) 1269–1276.
[46] A. Takawale, P. Zhang, V.B. Patel, X. Wang, G. Oudit, Z. Kassiri, Tissue inhibitor of matrix metalloproteinase-1 promotes myocardial fibrosis by mediating CD63-integrin beta1 interaction, Hypertension 69 (2017) 1092–1103.
[47] D. Fan, A. Takawale, R. Basu, V. Patel, J. Lee, V. Kandalam, et al., Differential role of TIMP2 and TIMP3 in cardiac hypertrophy, fibrosis, and diastolic dysfunction, Cardiovasc. Res. 103 (2014) 268–280.
[48] M. Tozakidou, D. Goltz, T. Hagenstrom, M.K. Budack, H. Vitzthum, K. Szlachta, et al., Molecular and functional remodeling of I(to) by angiotensin II in the mouse left ventricle, J. Mol. Cell. Cardiol. 48 (2010) 140–151.
[49] C. Marionneau, S. Brunet, T.P. Flagg, T.K. Pilgram, S. Demolombe, J.M. Nerbonne, Distinct cellular and molecular mechanisms underlie functional remodeling of repolarizing K+ currents with left ventricular hypertrophy, Circ. Res. 102 (2008) 1406–1415.
[50] A.M. De Jong, I.C. Van Gelder, I. Vreeswijk-Baudoin, M.V. Cannon, W.H. Van Gilst, A.H. Maass, Atrial remodeling is directly related to end-diastolic left ventricular pressure in a mouse model of ventricular pressure overload, PLoS One 8 (2013) e72651.
[51] A. Purohit, A.G. Rokita, X. Guan, B. Chen, O.M. Koval, N. Voigt, et al., Oxidized Ca2+/Calmodulin-dependent protein kinase II triggers atrial Fibrillation, Circulation 128 (2013) 1748–1757.
[52] P.D. Swaminathan, A. Purohit, T.J. Hund, M.E. Anderson, Calmodulin-dependent protein kinase II: linking heart failure and arrhythmias, Circ. Res. 110 (2012) 1661–1677.

Data Supplement

Supplemental Methods

Mice

Male wildtype mice were treated with saline or Ang II (3 mg/kg/day) for 3 weeks via osmotic minipumps (Alzet model 1004). To implant these osmotic pumps mice were anesthetized by isoflurane inhalation (2%). Osmotic pumps were inserted subcutaneously via a mid-scapular incision.

In vivo electrophysiology

A 1.2 French octapolar electrophysiology catheter containing 8 electrodes spaced 0.5 mm apart was used for intracardiac pacing experiments as we have described previously [1,2]. Inducibility of AF was studied using burst pacing in the right atrium [1,2]. We used 3 trains of 2 s burst pacing as follows: the first 2 s burst was given at a cycle length of 40 ms with a pulse duration of 5 ms. Following 3 min of stabilization a second 2 s burst was applied at a cycle length 20 ms with a pulse duration of 5 ms. After another 3 min of stabilization the final 2 s burst was given at a cycle length of 20 ms with a pulse duration of 10 ms. AF was defined as a rapid and irregular atrial rhythm (fibrillatory baseline in the ECG) with irregular RR intervals lasting at least 1 s on the surface ECG. All ECG data were acquired using a Gould ACQ-7700 amplifier and Ponemah Physiology Platform software (Data Sciences International) as we have described previously [1,2]. Body temperature was maintained at 37˚C using a heating pad.

High resolution optical mapping

To study patterns of electrical conduction in the mouse atria we used high resolution optical mapping in atrial preparations as we have done previously [2-4]. To isolate our atrial preparation mice were administered a 0.2 ml intraperitoneal injection of heparin (1000 IU/ml) to

prevent blood clotting and were then anesthetized by isoflurane inhalation and cervically dislocated. Hearts were excised into Krebs solution (35°C) containing (in mM): 118 NaCl, 4.7 KCl, 1.2 KH_2PO_4, 12.2 $MgSO_4$, 1 $CaCl_2$, 25 $NaHCO_3$, 11 glucose and bubbled with 95% O_2/5% CO_2 in order to maintain a pH of 7.4. The atria were dissected away from the ventricles and pinned in a dish with the epicardial surface facing upwards (towards the imaging equipment). The superior and inferior vena cavae were cut open so that the crista terminalis could be visualized and the preparation could be pinned out flat.

The atrial preparation was superfused continuously with Krebs solution (35°C) bubbled with 95% O_2/5% CO_2 and allowed to equilibrate for at least 30 min. During this time the preparation was treated with the voltage sensitive dye di-4-ANEPPS (10 µM) for ~15 min and blebbistatin (10 µM) was added to the superfusate to suppress contractile activity [5,6]. Blebbistatin was present throughout the duration of the experiments in order prevent motion artifacts during optical mapping.

Di-4-ANEPPS loaded atrial preparations were illuminated with light at a wavelength of 520 – 570 nM using an EXFO X-cite fluorescent light source (Lumen Dynamics). Emitted light (590 – 640 nM) was captured using a high speed EMCCD camera (Evolve 128, Photometrics). Data were captured from an optical field of view of 8 x 8 mm^2 at a frame rate of ~900 frames/s using Metamorph software (Molecular Devices). The spatial resolution was 67 x 67 µm for each pixel. Magnification was constant in all experiments and no pixel binning was used.

All optical data were analyzed using custom software written in Matlab. Pseudocolor electrical activation maps were generated from measurements of activation time at individual pixels as defined by assessment of dF/dt_{max}. In all cases background fluorescence was subtracted. Local conduction velocity (CV) was quantified specifically in the right atrial myocardium (within the right atrial appendage) and the left atrial myocardium (with in the left atrial appendage) using an established approach previously described [3,7,8]. Briefly, activation times at each pixel from a 7 x 7 pixel array were determined and fit to a plane using the least

squares fit method. The direction on this plane that is increasing the fastest represents the direction that is perpendicular to the wavefront of electrical propagation and the maximum slope represents the inverse of the speed of conduction in that direction. With a spatial resolution of 67 x 67 μM per pixel, the area of the 7 x 7 pixel array was 469 x 469 μM. Thus, using this method, we computed maximum local CV vectors in the atrial region of interest. Optical APs were assessed by measuring the change in fluorescence as a function of time at individual pixels within the right and left atria.

Isolation of mouse atrial myocytes

The procedures for isolating mouse atrial myocytes have been described previously [9,10] and were as follows. Mice were administered a 0.2 ml intraperitoneal injection of heparin (1000 IU/ml) to prevent blood clotting. Following this, mice were anesthetized by isoflurane inhalation and then sacrificed by cervical dislocation. The heart was excised into Tyrode's solution (35ºC) consisting of (in mM) 140 NaCl, 5.4 KCl, 1.2 KH_2PO_4, 1.0 $MgCl_2$, 1.8 $CaCl_2$, 5.55 glucose, and 5 HEPES, with pH adjusted to 7.4 with NaOH. The right or left atrial appendage was dissected from the heart and cut into strips, which were transferred and rinsed in a 'low Ca^{2+}, Mg^{2+} free' solution containing (in mM) 140 NaCl, 5.4 KCl, 1.2 KH_2PO_4, 0.2 $CaCl_2$, 50 taurine, 18.5 glucose, 5 HEPES and 1 mg/ml bovine serum albumin (BSA), with pH adjusted to 6.9 with NaOH. Atrial tissue was digested in 5 ml of 'low Ca^{2+}, Mg^{2+} free' solution containing collagenase (type II, Worthington Biochemical Corporation), elastase (Worthington Biochemical Corporation) and protease (type XIV, Sigma Chemical Company) for 30 min. Then the tissue was transferred to 2.5 ml of modified KB solution containing (in mM) 100 potassium glutamate, 10 potassium aspartate, 25 KCl, 10 KH_2PO_4, 2 $MgSO_4$, 20 taurine, 5 creatine, 0.5 EGTA, 20 glucose, 5 HEPES, and 0.1% BSA, with pH adjusted to 7.2 with KOH. The tissue was mechanically agitated using a wide-bore pipette. This procedure yielded individual right or left atrial myocytes that were stored in KB solution until experimental use within 6 hours of isolation.

Solutions and electrophysiological protocols

Stimulated action potentials (APs) were recorded using either the perforated patch-clamp technique or the whole cell patch-clamp technique. There were no differences in AP parameters between perforated and whole cell configurations. To record APs the recording chamber was superfused with a normal Tyrode's solution (22 – 23ºC) containing (in mM) 140 NaCl, 5 KCl, 1 $MgCl_2$, 1 $CaCl_2$, 10 HEPES, and 5 glucose, with pH adjusted to 7.4 with NaOH. The pipette filling solution contained (in mM) 135 KCl, 0.1 $CaCl_2$, 1 $MgCl_2$, 5 NaCl, 10 EGTA, 4 Mg-ATP, 6.6 Na-phosphocreatine, 0.3 Na-GTP and 10 HEPES, with pH adjusted to 7.2 with KOH. Amphotericin B (200 µg/ml) was added to this pipette solution to record APs with the perforated patch clamp technique.

For recording I_{Na} atrial myocytes were superfused with a modified Tyrode's solution (22 – 23°C) containing the following (in mM): 130 CsCl, 5 NaCl, 5.4 TEA-Cl, 1 $MgCl_2$, 1 $CaCl_2$, 10 HEPES, 5.5 glucose, (pH 7.4, adjusted with CsOH). Nitrendipine (10 µM) was added to the superfusate to block $I_{Ca,L}$. The pipette solution for I_{Na} contained (in mM): 120 CsCl, 5 NaCl, 1 $MgCl_2$, 0.2 $CaCl_2$, 10 HEPES, 5 MgATP, 0.3 Na-GTP, 5 BAPTA (pH 7.2, adjusted with CsOH). I_{Na} was recorded using 50 ms voltage clamp steps between -100 and 10 mV from a holding potential of -120 mV. A modified, sodium-free Tyrode's solution was used to recorded $I_{Ca,L}$. This solution contained (in mM): 145.5 TEA-Cl, 1 $MgCl_2$, 2 $CaCl_2$, 10 HEPES, and 5.5 glucose adjusted to pH 7.4 with CsOH. The internal pipette solution used to record $I_{Ca,L}$ contained (in mM): 135 CsCl, 5 NaCl, 1 $MgCl_2$, 0.2 $CaCl_2$, 5 EGTA, 0.3 Na-GTP, 4 Mg-ATP, 6.6 Na-phosophocreatine, and 10 HEPES adjusted to pH 7.2 with CsOH. The voltage clamp protocol used to record $I_{Ca,L}$ was a series of voltage clamp steps from -60 to +80 mV in 10 mV increments for 250 ms, returning to a holding potential of -70 mV between each step.

I_{Na} and $I_{Ca,L}$ activation kinetics were determined by calculating chord conductance (G) with the equation $G=I/(V_m-E_{rev})$, where V_m represents the depolarizing voltages and E_{rev} is the

reversal potential measured from the current-voltage relationships of $I_{Ca,L}$ or I_{Na}. Maximum conductance (G_{max}) and $V_{1/2}$ of activation for $I_{Ca,L}$ and I_{Na} were determined using the following function: $G=[(V_m-V_{rev})][G_{max}][-1/[(1+\exp((V_m-V_{1/2})/k))+1]]$.

Potassium currents (I_K) were recorded in the whole cell configuration using the normal Tyrode's solution and pipette solutions used to record APs. To record total potassium currents (no pre-pulse), cells were held at -80 mV then I_K was recorded using voltage clamp steps (500 ms duration) between -120 and +80 mV in 10 mV increments. To record potassium currents with an inactivating pre-pulse (to inactivate I_{to}), cells were given a 200 ms pre-pulse to -40 mV immediately followed by 500 ms voltage clamp steps from -120 to +80 mV from a holding potential of -80 mV. For these recordings with and without a pre-pulse recordings, I_K was measured at the peak current for each voltage step. I_{to} was calculated as the difference current between the recordings with and without a pre-pulse [11,12]. I_{to} activation kinetics were determined by calculating chord conductance from these difference current measurements, normalizing to maximum conductance, and fitting the data with a Boltzmann function.

I_{Kur}, as carried by Kv1.5 channels, was measured as the component of I_K sensitive to 4-aminopyradie (4-AP; 100 µM). The voltage clamp protocol for measuring I_{Kur} included a pre-pulse to -40 mV for 200 ms to inactivate I_{to} immediately followed by a 500 ms step to +30 mV before returning to a holding potential of -80 mV. Peak currents at baseline, in the presence of 4-AP, and after washout were measured.

Micropipettes were pulled from borosilicate glass (with filament, 1.5 mm OD, 0.75 mm ID, Sutter Instrument Company) using a Flaming/Brown pipette puller (model p-87, Sutter Instrument Company). The resistance of these pipettes was 4 – 8 MΩ when filled with recording solution. Micropipettes were positioned with a micromanipulator (Burleigh PCS-5000 system) mounted on the stage of an inverted microscope (Olympus IX71). Seal resistance was 2 – 15 GΩ. Rupturing the sarcolemma in the patch for voltage clamp experiments resulted in access resistances of 5 – 15 MΩ. Series resistance compensation averaged 80 – 85% using an

Axopatch 200B amplifier (Molecular Devices). For perforated patch clamp experiments access resistance was monitored for the development of capacitative transients upon sealing to the cell membrane with Amphotericin B in the pipette. Typically, access resistance became less than 25 MΩ within 5 min of sealing onto the cell, which was sufficient for recording stimulated APs in current clamp mode. Data were digitized using a Digidata 1440 and pCLAMP 10 software (Molecular Devices) and stored on computer for analysis. No junction potential corrections were applied in our analyses. All patch-clamp studies were conducted at room temperature, which must be noted when considering these results in the context of studies performed *in vivo*.

Western blotting

Protein samples were extracted from the right or left atrial appendage. Tissue was pre-cooled in liquid nitrogen, ground into a powder, and incubated in modified RIPA buffer (50 mM Tris, 150 mM NaCl, 25 mM sucrose, 1 mM EDTA, 1% Triton, 0.1% SDS) containing 0.5 mM DTT (1,4-Dithiothreitol, Roche) and Protease Inhibitor Cocktail (Sigma-Aldrich) for 1 hour on ice. Preparations were centrifuged at 10 000 rpm at 4ºC for 10 minutes. Protein concentrations were measured using a Bio-Rad *DC*™ Protein Assay Kit II (Bio-Rad Laboratories). Protein samples (20 µg/lane) were separated by 7.5% SDS-polyacrylamide gels (SDS-PAGE) and transferred onto a BioTrace™ NT Nitrocellulose Transfer Membrane (VWR). A protein concentration of 40 µg/lane and a 15% SDS-PAGE gel was used for KChIP2 western blot experiments. Next, the membrane was blocked with 1% casein in Tris-buffered saline (TBS; Bio-Rad Laboratories) for 1 hour and incubated a PKCα (1:500, Cell Signaling Technology), K_V4.2 (1:500, Alomone Labs), K_V4.3 (1:500, Alomone Labs), K_V1.5 (1:500, Alomone Labs), or KChIP2 (1:500, Alomone Labs) primary antibody overnight at 4ºC. The membrane was washed 3 times in TBST (TBS with 1% Tween 20 (Bio-Rad Laboratories)) and incubated with goat anti-rabbit IgG StarBright Blue 700 (1:5000, Bio-Rad Laboratories) and hFAB Rhodamine Anti-GAPDH IgG (1:3000, Bio-Rad

Laboratories) for 1 hour at room temperature. The membrane was washed 3 times with 1% TBST then imaged using the ChemiDoc™ MP Imaging System (Bio-Rad Laboratories).

Quantitative PCR

Total RNA was isolated from right or left atrial appendages using a PureZOL™ RNA Isolation Reagent and the Aurum™ Total RNA Fatty and Fibrous Tissue Kit (Bio-Rad Laboratories) as per kit instructions. RNA samples were eluted from the spin column in 40 µL elution buffer. RNA yield and purity were assessed using a Nanodrop. All samples had a A_{260}/A_{280} of over 2.0 and therefore were free of DNA contamination. RNA integrity was assessed by observing 28S and 18S rRNA subunits using the Experion RNA StdSens Analysis Kit (Bio-Rad Laboratories). Next, cDNA (20 ng/µL) was synthesized using the iScript™ cDNA Synthesis Kit (Bio-Rad Laboratories). Reactions were performed in a Bio-Rad MyCycler thermal cycler using the following protocol: 5 min of priming at 25ºC followed by reverse transcription for 30 min at 42ºC then 5 min at 85ºC to inactivate reverse transcriptase.

All qPCR reactions were run in duplicate in 10 µL reactions that contained the following: 4 µL sample cDNA, 5.6 µL GoTaq® qPCR Master Mix (Promega), and 0.4 µL primers. Primers were reconstituted to a final concentration of 100 µM with nuclease free water and stored at -20ºC until use. Primers were diluted to 10 µM for qPCR reactions. RT-qPCR reactions were performed using the CFX386 Touch™ Real-Time PCR Detection System (Bio-Rad) using the following protocol: Taq polymerase was activated for 2 min at 95ºC followed by 39 cycles of denaturing for 15 s at 95ºC, annealing for 30 s at 60ºC, and extension for 30s at 72ºC. This was followed by melt curve analysis from 65-95ºC in 0.5ºC increments. Data were analyzed using the $2^{-\Delta\Delta C_T}$ method using the CFX Manager Software version 3.1 (Bio-Rad). Gene expression was normalized to GAPDH and β-actin. Primer sequences are listed in Supplemental Table 10 below.

Supplemental Figures

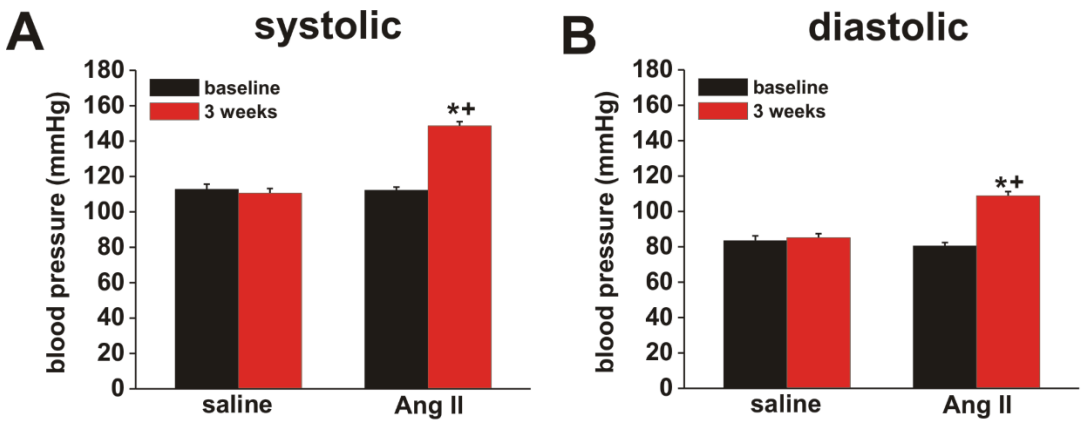

Supplemental Figure S1. Blood pressure in mice treated with Ang II. Measurements of systolic (**A)** and diastolic (**B**) blood pressure at baseline and following 3 weeks of saline or Ang II treatment. *P<0.05 vs. baseline within treatment group, ^{+}P<0.05 vs. saline at 3 week time point by two-way ANOVA with Tukey's posthoc test, n=16 mice for saline and 17 mice for Ang II.

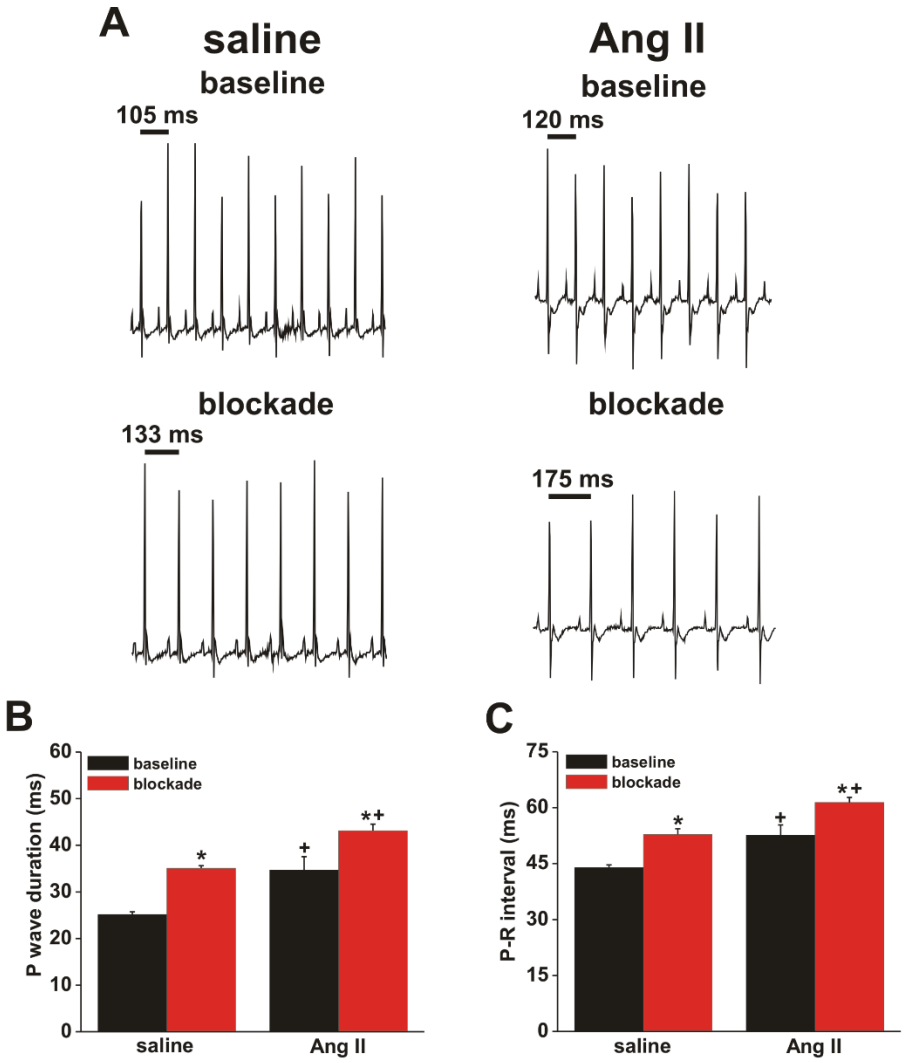

Supplemental Figure S2. Effects of autonomic nervous system blockade on P wave duration and P-R interval in mice treated with Ang II. A, Representative ECGs in anesthetized mice treated with saline or Ang II at baseline and after an intraperitoneal injection of atropine and propranolol to block the autonomic nervous system. **B,** Summary of the effects of autonomic blockade on P wave duration in saline and Ang II treated mice. **C,** Summary of the effects of autonomic blockade on P-R interval in saline and Ang II treated mice. **P*<0.05 vs. baseline, $^{+}$*P*<0.05 vs. saline by two-way ANOVA with Tukey's posthoc test, *n*=6 saline and 11 Ang II treated mice.

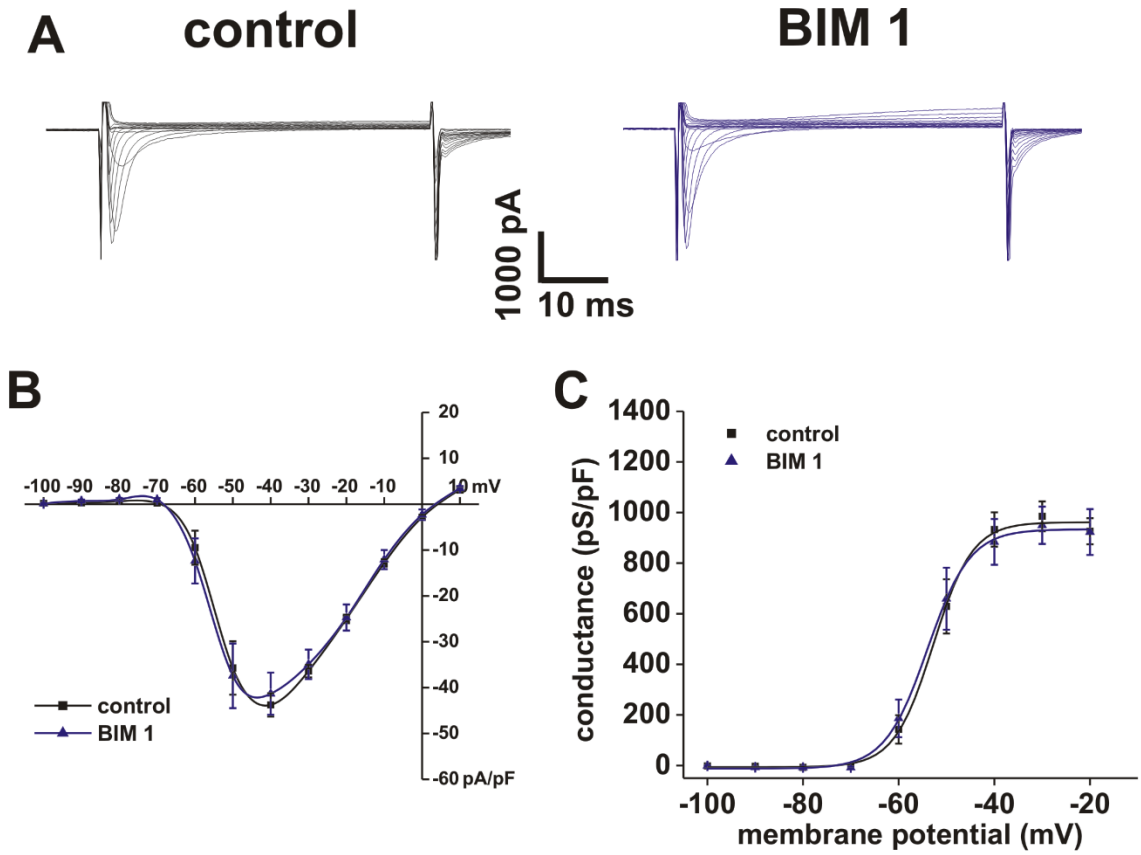

Supplemental Figure S3. Effects of protein kinase C inhibition on I_{Na} in saline treated mice. A, Representative I_{Na} recordings in saline treated left atrial myocytes in control conditions and after dialysis with the PKC inhibitor BIM 1 (1 µM). Cell capacitances for representative recordings are 49 pF for control and 57 pF for BIM 1. Voltage clamp protocol is as shown in Figure 5A. **B,** Summary I_{Na} IV curves in control conditions and after BIM1 application in left atrial myocytes isolated from saline treated mice. **C,** Summary I_{Na} activation curves in control conditions and after application of BIM 1 for left atrial myocytes isolated from saline treated mice. There were no effects of BIM 1 on I_{Na} density (P=0.94) or I_{Na} conductance (P=0.96) in saline treated mice; data analyzed by two-way repeated measures ANOVA with Tukey's posthoc test; n=7 myocytes for control and 6 for BIM 1. Refer to Supplemental Table 8 for a summary of I_{Na} activation kinetics.

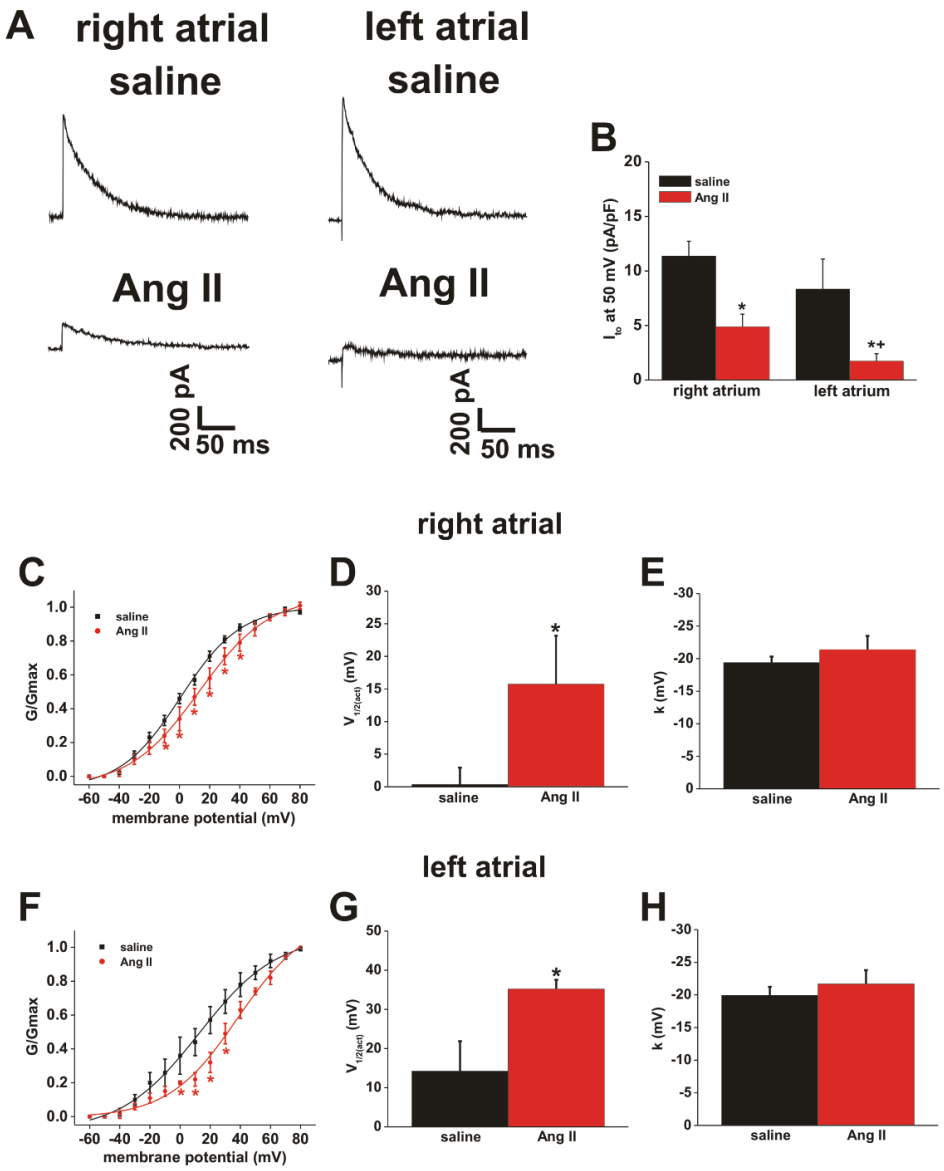

Supplemental Figure S4. Comparison of the effects of Ang II on I_{to} in right and left atria. **A,** Representative I_{to} recordings at +50 mV in right and left atrial myocytes from mice treated with saline or Ang II. Cell capacitances for representative recordings are as follows. Right atrial/saline: 50.7 pF; right atrial/Ang II: 40 pF; left atrial/saline: 52.2: left atrial/Ang II: 110.1 pF. **B,** Summary of I_{to} density at +50 mV in right and left atrial myocytes from saline and Ang II treated mice. **P*<0.05 vs. saline, $^{+}$*P*<0.05 vs. right atrium by two-way ANOVA with Tukey's posthoc test, *n*=17 right atrial/saline myocytes, 19 right atrial/Ang II myocytes, 10 left atrial/saline myocytes and 17 left atrial/Ang II myocytes. **C,** I_{to} activation curves for right atrial myocytes. **P*<0.05 vs. saline by two-way ANOVA with Tukey's posthoc test; *n*=16 saline and 15 Ang II treated myocytes. **D,** Summary of the effects of Ang II on I_{to} $V_{1/2(act)}$ in right atrial myocytes. **P*<0.05 by Student's *t*-test. **E,** Summary of the effects of Ang II on I_{to} slope factor (k) in right atrial myocytes. **F,** I_{to} activation curves for left atrial myocytes. **P*<0.05 vs. saline by two-way ANOVA with Tukey's posthoc test; *n*=7 saline and 7 Ang II treated myocytes. **G,** Summary of the effects of Ang II on I_{to} $V_{1/2(act)}$ in left atrial myocytes. **P*<0.05 by Student's *t*-test. **H,** Summary of the effects of Ang II on I_{to} slope factor (k) in left atrial myocytes.

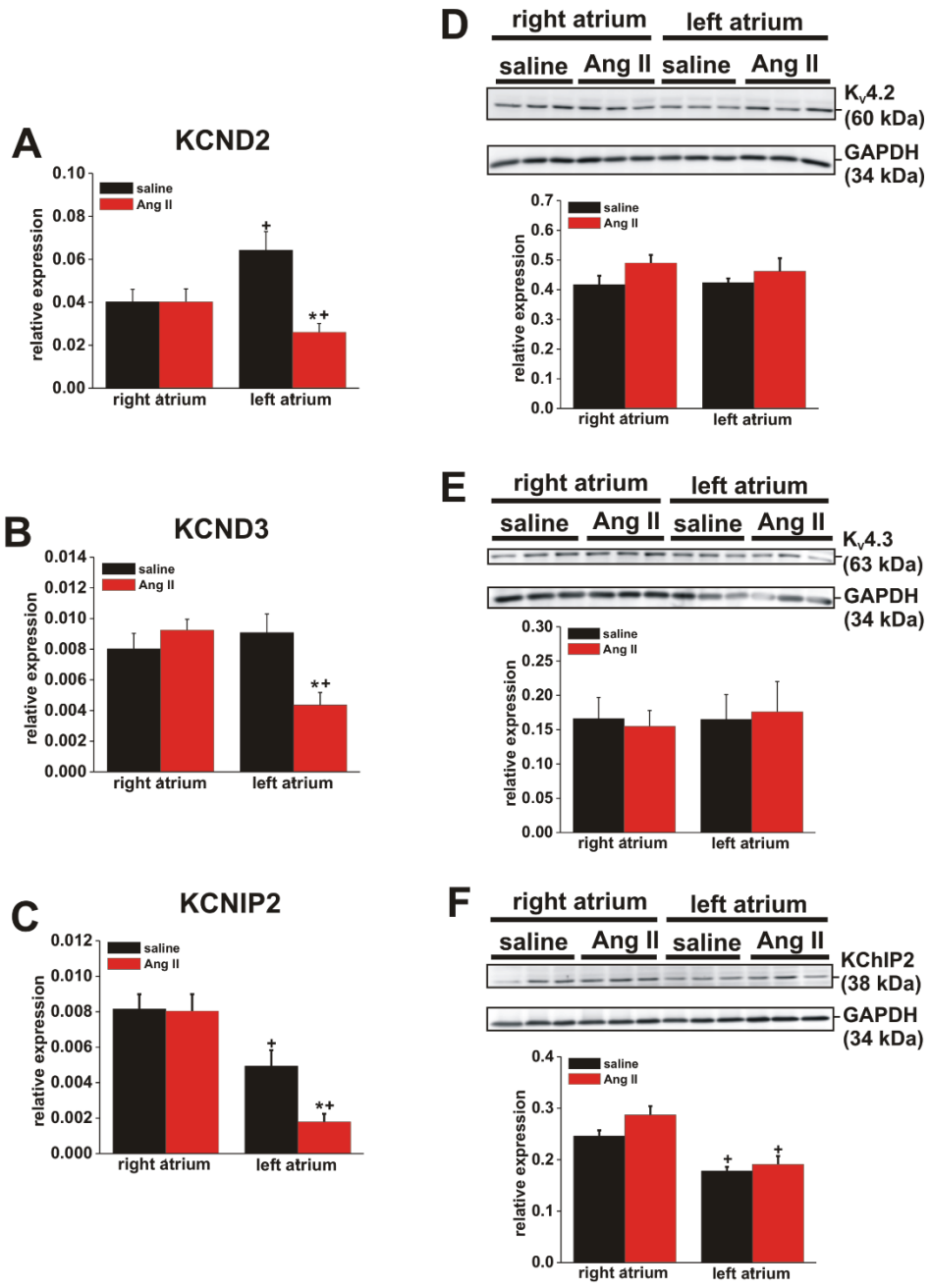

Supplemental Figure S5. Effects of Ang II on potassium channel gene and protein expression in the right and left atria. A-C, mRNA expression of KCND2 (**A**), KCND3 (**B**) and KCNIP2 (**C**) in right and left atria from saline and Ang II treated mice. **P*<0.05 vs. saline, $^{+}$*P*<0.05 vs. right atrium. Ang II had no effect on expression of KCND2 (*P*=1.000), KCND3 (*P*=0.384) or KCNIP2 (*P*=0.923) in the right atrium. Data analyzed by two-way ANOVA with Tukey's posthoc test, *n*=7 for right atrium/saline, 8 for right atrium/Ang II, 8 for left atrium/saline and 8 for left atrium/Ang II. **D-E,** Protein expression of K_V4.2 (**D**), K_V4.3 (**E**) and KChIP2 (**F**) in right and left atria from saline and Ang II treated mice. Ang II had no effect on expression of K_V4.2 (*P*=0.084), K_V4.3 (*P*=0.995) or KChIP2 (*P*=0.070) in the right or left atria. Data analyzed by two-way ANOVA with Tukey's posthoc test; *n*=6 for each group.

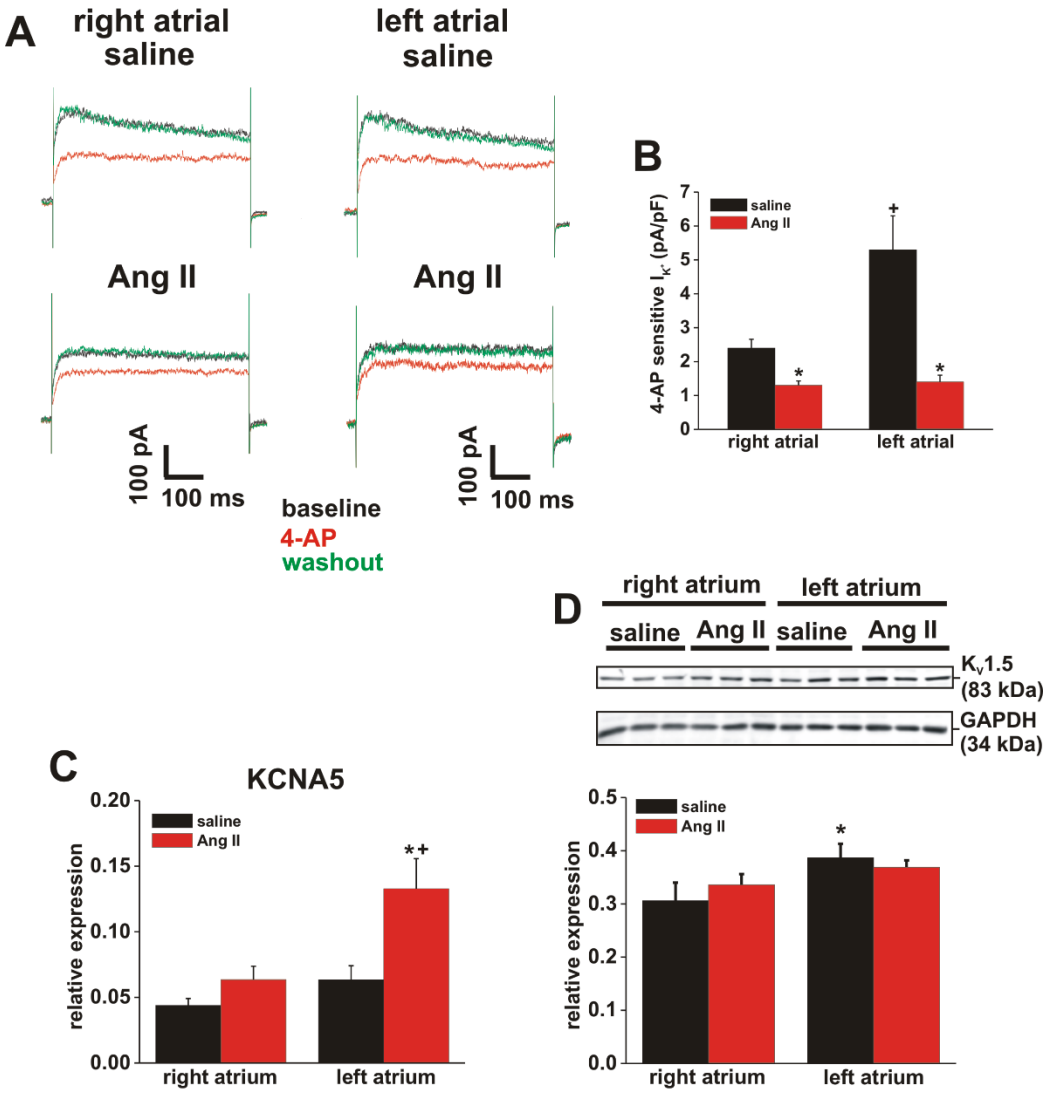

Supplemental Figure S6: Effects of Ang II I_{Kur} in right and left atria. A, Representative I_K recordings at +30 mV illustrating the effects of 4-AP (100 µM), which inhibits $K_V1.5$ mediated K^+ current, in right and left atrial myocytes from mice treated with saline or Ang II. Cell capacitances for representative recordings are as follows. Right atrial/saline: 33.8 pF; right atrial/Ang II: 67 pF; left atrial/saline: 35.5 pF; left atrial/Ang II: 66.6 pF. **B,** Summary of the effects of Ang II on amplitude of the 4-AP sensitive K^+ current. **P*<0.05 vs. saline; $^+$*P*<0.05 vs. right atrial by two-way ANOVA with Tukey's posthoc test; *n*=20 myocytes for right atrial/saline, 14 for right atrial/Ang II, 12 for left atrial/saline and 9 for left atrial/Ang II. **C,** mRNA expression of KCNA5 in right and left atria from saline and Ang II treated mice. **P*<0.05 vs. saline; $^+$*P*<0.05 vs. right atrium by two-way ANOVA with Tukey's posthoc test; *n*=7 for right atrium/saline, 8 for right atrium/Ang II, 8 for left atrium/saline and 8 for left atrium/Ang II. **D,** Protein expression of $K_V1.5$ in the right and left atria from saline and Ang II treated mice. **P*<0.05 vs right atrium. Ang II had no effect of $K_V1.5$ expression in right (*P*=0.38) or left (*P*=0.60) atria. Data analyzed by two-way ANOVA with Tukey's posthoc test; *n*=9 samples for each group.

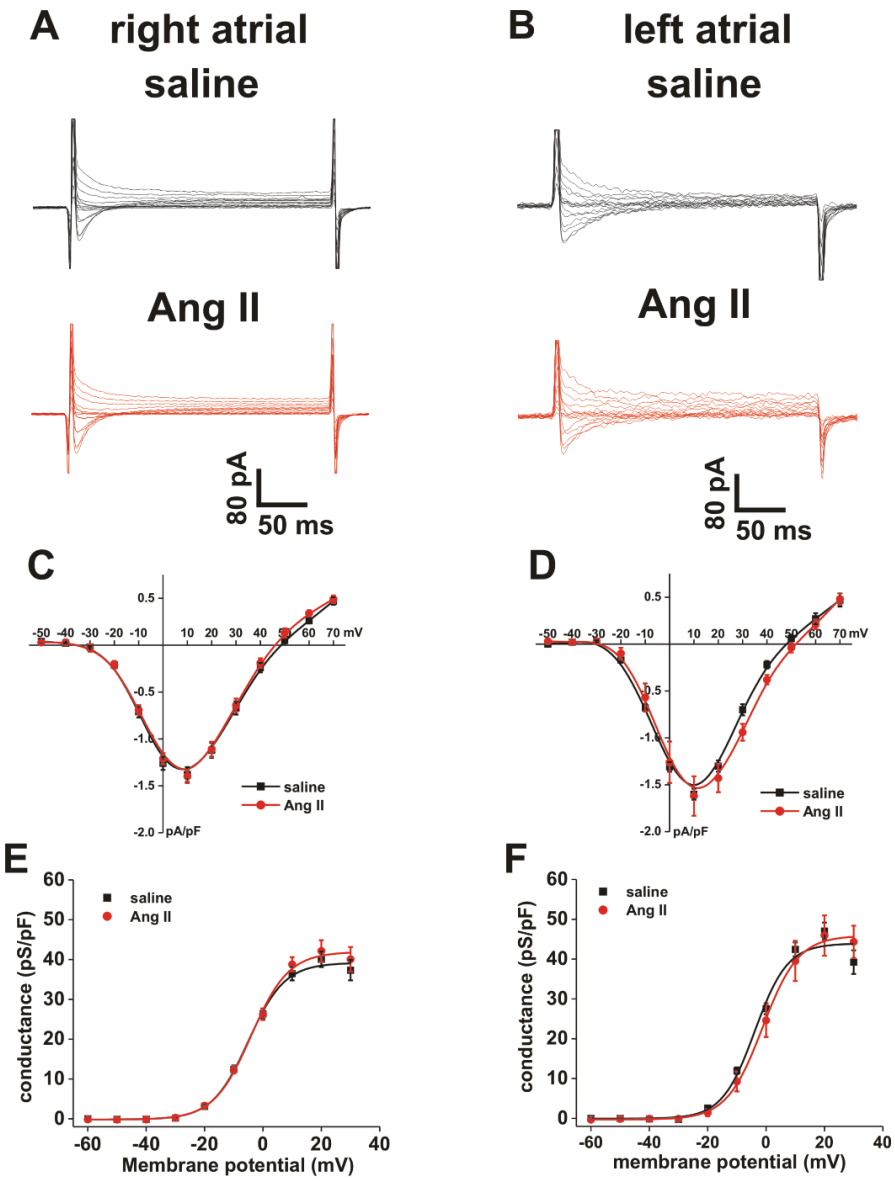

Supplemental Figure S7. Effects of Ang II treatment on atrial calcium current. A and B, Representative $I_{Ca,L}$ recordings in right (**A**) and left (**B**) atrial myocytes from saline and Ang II treated mice. Cell capacitances for representative recordings are as follows. Right atrial/saline: 37.6 pF; right atrial/Ang II: 46.4 pF; left atrial/saline: 53.5; left atrial/Ang II: 64.9 pF. **C and D,** Summary $I_{Ca,L}$ IV curves in right (**C**) and left (**D**) atrial myocytes from saline and Ang II treated mice. Ang II had no effect on $I_{Ca,L}$ density in right (P=0.53) or left (P=0.80) atrial myocytes by two-way repeated measures ANOVA with Tukey's posthoc test. **E and F,** Summary $I_{Ca,L}$ activation curves in right (**E**) and left (**F**) atrial myocytes from saline and Ang II treated mice. Ang II had no effect on $I_{Ca,L}$ conductance in right (P=0.52) or left (P=0.78) atrial myocytes by two-way repeated measures ANOVA with Tukey's posthoc test, n=13 myocytes for right atrial/saline, 15 for right atrial/Ang II, 11 for left atrial/saline and 10 for left atrial/Ang II. Refer to Supplemental Table 9 for a summary of $I_{Ca,L}$ activation kinetics.

Supplemental Table 1: Echocardiographic measurements in mice treated with Ang II for 3 weeks

	baseline	Ang II	*P* value
LVAWd (mm)	0.72 ± 0.06	1.01 ± 0.02*	0.008
LVPWd (mm)	0.85 ± 0.09	0.91 ± 0.04	0.39
LVIDd (mm)	4.15 ± 0.18	4.09 ± 0.13	0.84
LVAWs (mm)	1.26 ± 0.06	1.01 ± 0.02*	0.02
LVPWs (mm)	1.35 ± 0.13	1.40 ± 0.12	0.76
LVIDs (mm)	2.98 ±0.08	2.40 ± 0.20*	0.03
EF (%)	58.8 ± 1.7	64.8 ± 7.9	0.66
LA $area_{max}$ (mm^2)	5.64 ± 0.29	8.64 ± 1.07*	0.02
LA $area_{min}$ (mm^2)	3.23 ± 0.35	6.80 ± 1.14*	0.03

LVAW, left ventricular anterior wall thickness; LVPW, left ventricular posterior wall thickness; LVID, left ventricular internal diameter. LVAW, LVPW and LVID measurements were made during systole (s) and diastole (d). EF, ejection fraction; LA $area_{max}$, maximum left atrial area; LA $area_{min}$, minimum left atrial area. Data are means ± SEM; *n*=5 mice; **P*<0.05 vs. baseline by Student's *t*-test.

Supplemental Table 2: Duration of arrhythmia in saline and Ang II treated mice that were induced into atrial fibrillation

	saline	Ang II
< 5s	100% (1/1)	43% (3/7)
5-30 s	0%	43% (3/7)
>30 s	0%	14% (1/7)

Numbers in parentheses indicate the number of mice in each group.

Supplemental Table 3: ECG intervals in mice treated with saline or Ang II

	saline	Ang II	*P* value
Heart rate (beats/min)	553 ± 8	513 ± 12*	0.01
R-R interval (ms)	108.8 ± 1.4	118.3 ± 3.1*	0.03
P wave (ms)	25.3 ± 0.6	32.6 ± 0.9*	<0.001
P-R interval (ms)	43.3 ± 0.8	51.4 ± 1.3*	0.003
P-R segment (ms)	18.2 ± 0.9	17.0 ± 1.2	0.86
AERP	29.0 ± 0.4	34.4 ± 1.3*	0.002
AVERP	49.4 ± 1.6	57.3 ± 2.5*	0.04

P-R interval measured from beginning of P wave to R wave. P-R segment measured from end of P wave to R wave. Data are means ± SEM; *n* = 15 saline and 18 Ang II treated mice. **P*<0.05 vs. saline by Student's *t*-test.

Supplemental Table 4: Action potential parameters in right atrial myocytes from mice treated with saline or Ang II

	saline	Ang II	*P* value
RMP (mV)	-78.6 ± 0.5	-78.9 ± 0.6	0.74
V_{max} (V/s)	150.6 ± 5.2	143.2 ± 5.7	0.35
OS (mV)	67.4 ± 2.9	63.7 ± 3.8	0.45
APD_{20} (ms)	1.7 ± 0.2	3.3 ± 0.5	<0.001
APD_{50} (ms)	10.3 ± 1.4	21.2 ± 3.2*	0.004
APD_{70} (ms)	23.7 ± 3.6	42.9 ± 5.8*	0.006
APD_{90} (ms)	54.6 ± 6.3	84.0 ± 7.2*	0.005

RMP, resting membrane potential; V_{max}, AP upstroke velocity; OS, overshoot; APD_{20}, AP duration at 20% repolarization; APD_{50}, AP duration at 50% repolarization; APD_{70}, AP duration at 70% repolarization; APD_{90}, AP duration at 90% repolarization. *P<0.05 vs. saline by Student's *t*-test; *n*=14 for saline and 12 for Ang II.

Supplemental Table 5: Action potential parameters in left atrial myocytes from mice treated with saline or Ang II

	saline	Ang II	*P* value
RMP (mV)	-77.6 ± 0.7	-77.4 ± 1.0	0.91
V_{max} (V/s)	146.7 ± 9.0	115.6 ± 7.5*	0.01
OS (mV)	67.2 ± 3.7	51.7 ± 3.3*	0.004
APD_{20} (ms)	1.5 ± 0.2	5.7 ± 1.1	<0.001
APD_{50} (ms)	7.9 ± 0.7	30.5 ± 4.3*	<0.001
APD_{70} (ms)	14.5 ± 1.5	61.6 ± 6.2*	<0.001
APD_{90} (ms)	44.6 ± 3.6	117.5 ± 7.7*	<0.001

RMP, resting membrane potential; V_{max}, AP upstroke velocity; OS, overshoot; APD_{20}, AP duration at 20% repolarization; APD_{50}, AP duration at 50% repolarization; APD_{70}, AP duration at 70% repolarization; APD_{90}, AP duration at 90% repolarization. *P<0.05 vs. saline by Student's *t*-test; *n*=14 for saline and 15 for Ang II.

Supplemental Table 6: I_{Na} kinetics in right and left atrial myocytes from Ang II treated mice

	G_{max} (pS/pF)	*P* value	$V_{1/2(act)}$ (mV)	*P* value	k (mV)	*P* value
right atrial saline (*n*=13)	1316.7 ± 17.1	0.22	-50.5 ± 0.5	0.30	4.3 ± 0.1	0.53
right atrial Ang II (*n*=12)	1270.0 ± 19.2		-49.6 ± 0.7		3.1 ± 0.6	
left atrial saline (*n*=17)	1236.2 ± 8.6	<0.001	-53.5 ± 0.9	0.03	3.0 ± 0.3	0.07
left atrial Ang II (*n*=18)	827.1 ± 13.1*		-50.6 ± 0.9*		3.8 ± 0.2	

G_{max}, maximum conductance, $V_{1/2(act)}$, voltage at which 50% of channels are activated; k, slope factor. **P*<0.05 vs. control value as indicated in the table cell immediately above, *n* values are as indicated in parentheses for each group. Data analyzed by Student's *t*-test.

Supplemental Table 7: Effects of PKC inhibition on I_{Na} kinetics in left atrial myocytes from Ang II treated mice

	G_{max} (pS/pF)	$V_{1/2(act)}$ (mV)	k (mV)
saline (*n*=12)	1154.6 ± 13.4	-54.4 ± 1.1	2.7 ± 0.4
Ang II (*n*=14)	843.2 ± 14.3*	-49.9 ± 0.9*	3.9 ± 0.2*
Ang II + BIM 1 (*n*=10)	1048.8 ± 11.9^{+}	-54.0 ± 1.5^{+}	3.1 ± 0.2

G_{max}, maximum conductance, $V_{1/2(act)}$, voltage at which 50% of channels are activated; k, slope factor. **P*<0.05 vs. saline, $^{+}$*P*<0.05 vs. Ang II, *n* values are as indicated in parentheses for each group. Data analyzed by one way ANOVA with Tukey's posthoc test.

Supplemental Table 8: Effects of PKC inhibition on I_{Na} kinetics in left atrial myocytes from saline treated mice

	G_{max} (pS/pF)	$V_{1/2(act)}$ (mV)	k (mV)
Control (*n*=7)	972.0 ± 54.5	-52.8 ± 1.7	2.8 ± 0.6
BIM1 (*n*=6)	948.9 ± 79.0	-53.6 ± 2.0	3.2 ± 0.4

G_{max}, maximum conductance, $V_{1/2(act)}$, voltage at which 50% of channels are activated; k, slope factor. BIM 1 had no effect on G_{max} (*P*=0.81), $V_{1/2(act)}$ (*P*=0.78) or k (*P*=0.64); data analyzed by Student's *t*-test, *n* values are as indicated in parentheses for each group.

Supplemental Table 9: $I_{Ca,L}$ kinetics in right and left atrial myocytes from Ang II treated mice

	G_{max} (pS/pF)	*P* value	$V_{1/2(act)}$ (mV)	*P* value	k (mV)	*P* value
right atrial saline (*n*=13)	40.6 ± 1.9	0.24	-5.1 ± 0.9	0.38	6.3 ± 0.4	0.68
right atrial Ang II (*n*=15)	42.2 ± 2.7		-3.6 ± 1.3		6.8 ± 0.6	
left atrial saline (*n*=11)	47.0 ± 2.2	0.81	-3.2 ± 1.0	0.15	6.0 ± 0.4	0.86
left atrial Ang II (*n*=10)	45.9 ± 5.1		-1.8 ± 1.0		6.0 ± 0.3	

G_{max}, maximum conductance, $V_{1/2(act)}$, voltage at which 50% of channels are activated; k, slope factor. **P*<0.05 vs control value as indicated in the table cell immediately above, *n* values are as indicated in parentheses for each group. Data analyzed by Student's *t*-test.

Supplemental Table 10: Quantitative PCR primers

Gene	Gene product	Primer Sequence (5'→ 3')	Amplicon length (bp)
SCN5a	$Na_V1.5$	Forward: GGAGTACGCCGACAAGATGT Reverse: ATCTCGGCAAAGCCTAAGGT	171
KCND2	$K_V4.2$	Forward: GCAAGCGGAATGGGCTAC Reverse: TGGTTTTCTCCAGGCAGTG	126
KCND3	$K_V4.3$	Forward: CCTAGCTCCAGCGGACAAGA Reverse: CCACTTACGTTGAGGACGATCA	60
KCNIP2	KChIP2	Forward: AACTATCCACGGTGTGCCAC Reverse: GGACATTCGTTCTTGAAGCCT	112
KCNA5	$K_V1.5$	Forward: TTATTCTTATGGCTGACGAGTGC Reverse: AAGGCACCAATAGTACATCCCAG	204
Col1a2	Collagen type I	Forward: GCGGACTCTGTTGCTGCTTGC Reverse: GACCTGCGGGACCCCTTTGT	125
Col3a1	Collagen type III	Forward: AGATCCGGGTCCTCCTGGCATTC Reverse: CTGGTCCCGGATAGCCACCCAT	194
TGFβ	TGFβ	Forward: CGAGGTGACCTGGGCACCATCCATGAC Reverse: CTGCTCCACCTTGGGCTTGCGACCCAC	405
MMP2	MMP2	Forward: CCACGTGACAAGCCCATGGGGCCC Reverse: GCAGCCTAGCCAGTCGGATTTGATG	486
MMP9	MMP9	Forward: TCGCGTGGATAAGGAGTTCTC Reverse: ATGGCAGAAATAGGCTTTGTCTTG	82
TIMP1	TIMP1	Forward: CAGATACCATGATGGCCCCC Reverse: CGCTGGTATAAGGTGGTCTCG	190
TIMP2	TIMP2	Forward: CCAGAAGAAGAGCCTGAACCA Reverse: GTCCATCCAGAGGCACTCATC	112
TIMP3	TIMP3	Forward: GGCCTCAATTACCGCTACCA Reverse: CTGATAGCCAGGGTACCCAAAA	135
TIMP4	TIMP4	Forward: TGCAGAGGGAGAGCCTGAA Reverse: GGTACATGGCACTGCATAGCA	80
GAPDH	GAPDH	Forward: AATGGGGTGAGGCCGGTGCT Reverse: CACCCTTCAAGTGGGCCCCG	87
β-*actin*	β-actin	Forward: CACCCTTCAAGTGGGCCCCG Reverse: CACCCTTCAAGTGGGCCCCG	227

References

[1] Egom EE, Vella K, Hua R, Jansen HJ, Moghtadaei M, Polina I, et al. Impaired sinoatrial node function and increased susceptibility to atrial fibrillation in mice lacking natriuretic peptide receptor C. J. Physiol. 2015;593:1127-46.

[2] Jansen HJ, Moghtadaei M, Mackasey M, Rafferty SA, Bogachev O, Sapp JL, et al. Atrial structure, function and arrhythmogenesis in aged and frail mice. Sci. Rep. 2017;7:44336.

[3] Azer J, Hua R, Krishnaswamy PS, Rose RA. Effects of natriuretic peptides on electrical conduction in the sinoatrial node and atrial myocardium of the heart. J. Physiol. 2014;592:1025-45.

[4] Hua R, MacLeod SL, Polina I, Moghtadaei M, Jansen HJ, Bogachev O, et al. Effects of Wild-Type and Mutant Forms of Atrial Natriuretic Peptide on Atrial Electrophysiology and Arrhythmogenesis. Circ. Arrhythm. Electrophysiol. 2015;8:1240-54.

[5] Fedorov VV, Lozinsky IT, Sosunov EA, Anyukhovsky EP, Rosen MR, Balke CW, et al. Application of blebbistatin as an excitation-contraction uncoupler for electrophysiologic study of rat and rabbit hearts. Heart Rhythm. 2007;4:619-26.

[6] Farman GP, Tachampa K, Mateja R, Cazorla O, Lacampagne A, de Tombe PP. Blebbistatin: use as inhibitor of muscle contraction. Pflugers Arch. 2008;455:995-1005.

[7] Nygren A, Lomax AE, Giles WR. Heterogeneity of action potential durations in isolated mouse left and right atria recorded using voltage-sensitive dye mapping. Am. J. Physiol. Heart Circ. Physiol. 2004;287:H2634-43.

[8] Morley GE, Vaidya D, Samie FH, Lo C, Delmar M, Jalife J. Characterization of conduction in the ventricles of normal and heterozygous Cx43 knockout mice using optical mapping. J. Cardiovasc. Electrophysiol. 1999;10:1361-75.

[9] Springer J, Azer J, Hua R, Robbins C, Adamczyk A, McBoyle S, et al. The natriuretic peptides BNP and CNP increase heart rate and electrical conduction by stimulating ionic currents in the sinoatrial node and atrial myocardium following activation of guanylyl cyclase-linked natriuretic peptide receptors. J. Mol. Cell. Cardiol. 2012;52:1122-34.

[10] Hua R, Adamczyk A, Robbins C, Ray G, Rose RA. Distinct patterns of constitutive phosphodiesterase activity in mouse sinoatrial node and atrial myocardium. PLoS One. 2012;7:e47652.

[11] Lomax AE, Kondo CS, Giles WR. Comparison of time- and voltage-dependent K+ currents in myocytes from left and right atria of adult mice. Am. J. Physiol. Heart Circ. Physiol. 2003;285:H1837-48.

[12] Kuo HC, Cheng CF, Clark RB, Lin JJ, Lin JL, Hoshijima M, et al. A defect in the Kv channel-interacting protein 2 (KChIP2) gene leads to a complete loss of I(to) and confers susceptibility to ventricular tachycardia. Cell. 2001;107:801-13.